Barremian-Aptian-Albian carbon isotope segments as chronostratigraphic signals: Numerical age calibration and durations

R. W. Scott
Precision Stratigraphy Associates and The University of Tulsa,
149 West Ridge Road, Cleveland Oklahoma 74020, USA
email: rwscott@cimtel.net

ABSTRACT: Chemostratigraphic signals are becoming common tools in chronostratigraphic correlations. Specifically total organic and carbonate carbon percentages ($TOC_{org/carb}$) and carbon isotope curves are diagnostic in Cretaceous Aptian-Albian-Cenomanian strata. Cretaceous carbon isotope signals define oceanic anoxic events (OAEs) and have been subdivided into successive segments. These segments are used as correlation markers because they represent oceanographic and depositional conditions, and hence, incur time significance. Although the segments have been integrated with biovents in key sections, numerical ages of the segments have yet to be calibrated. Because direct correlation of these segments of carbon isotope curves with interbedded radiometrically dated beds is not possible currently, other methods must be applied to interpolate numerical ages. Graphic plots of five sections successfully integrate carbon isotope segments with established numerically dated chronostratigraphic markers. Carbon isotope segments were first defined in European Tethys Cismon and Rotter Sattel Barremian-Albian sections. The Aptian segments were subsequently identified in the Mexican Santa Rosa Canyon section where the lower Albian segments were defined. Each section has well documented microfossils and magnetochrons that relate the segments to biozones. These bioevents and chronozones enable the carbon segments to be integrated with a comprehensive Cretaceous time scale, the CRECSDB42. Ages assigned to the segments enable them to be used in sections where local fossil zones are recorded such as in the Chihuahua basin in northern Mexico. The age calibration of carbon isotope segments measures the durations of the oceanic isotopic excursions. The durations fluctuate up to and after OAE 1a at irregular frequencies different from climatic cycles. Changing durations of carbon isotope segments may be clues to changes in processes or the effects of the process that altered the ocean carbon reservoir in addition to climatic changes.

Key words: Carbon isotope chemostratigraphy, Barremian, Aptian, Albian, Tethys

INTRODUCTION

Chemostratigraphic signals have become common, widespread tools in chronostratigraphic correlations (Jarvis et al. 2006; Jenkyns 2010; Di Lucia et al. 2012) because they are "linked directly to the biosphere and the global carbon cycle" (Saltzman and Thomas 2014). If chemostratigraphy is integrated with chronostratigraphic data from biostratigraphy and magnetostratigraphy, it becomes a reliable tool for correlation (Weissert et al. 2008). The two most widely used chemostratigraphic signals are those of total organic carbon (TOC) and the $\delta^{13}C$ ppm of bulk carbonate. Total organic carbon percentages in organic-rich sedimentary rocks ($TOC_{org/carb}$) are named lithostratigraphic units, such as "Livello Selli" in the Italian Apennines (Menegatti et al. 1998). One hypothesis posits that such deposits represent 'biocalcification crises', which were "times of reduced calcification rates…causing widespread carbonate platform collapse…" (Weissert and Erba 2004). These events affected the global carbon isotope budget. As a result, the $\delta^{13}C$ signal of both pelagic and shelf limestone fluctuated. An alternative hypothesis is that orbitally-induced climate changes controlled sea level and terrestrial erosion so that alternating organic-rich deposits were dominated by either oceanic or terrestrial organic matter (Erbacher et al. 1996).

During much of the Albian, carbon isotope fluctuations corresponded to the ~400 kyr orbital cycle recorded in pelagic mudstones of the Marne a Fucoidi Formation, Central Apennines, Italy (Giorgioni et al. 2012). These researchers proposed that carbon isotope fluctuations were related to periods of stronger and weaker contrasting monsoon seasons. Lower $\delta^{13}C$ measurements correspond to greater seasonal contrasts and higher isotope peaks relate to eccentricity minima with weaker climate contrast. Cretaceous ocean circulation may have been driven by deep eddies that influenced seasonal monsoons (Hay 2007). Stronger ocean eddies and stronger monsoon seasons may have reduced the rate of organic carbon burial thus decreasing oceanic carbon isotope composition. Stronger monsoons would increase weathering and erosion resulting increased influx of light carbon from continental plants. Weaker eddies and monsoonal seasons would increase burial rates of organic carbon and decrease erosion resulting in increased in $\delta^{13}C$. For example black shale with high terrestrial matter correspond with eccentricity maxima and pelagic marine red beds, which reflect oxygenated bottom waters (Hu et al. 2012) correspond with eccentricity minima (Giorgioni et al. 2012, fig. 4).

The isotopic variations of total bulk inorganic carbon in carbonate strata have been divided into successive carbon isotope segments (C). Carbon and oxygen isotope curves are now documented in many pelagic and shelf Cretaceous sections (Jenkyns et al. 1994; Leckie et al. 2002; Weissert and Erba 2004; Herrle et al. 2004; Wissler et al. 2003; Stein et al. 2011; Di Lucia

et al. 2012; Giorgioni et al. 2012; Saltzman and Thomas et al. 2012; Gamacorta et al. 2015). These segments are used as correlation markers because they represent oceanographic and depositional conditions, and hence, incur time significance (Menegatti et al. 1998; Wissler et al. 2002; Wissler et al. 2003; Föllmi et al. 2006; Burla et al. 2008). The most dramatic isotope peaks were initially identified in organic-rich black shale deposits and define oceanic anoxic events (OAEs). The proportions of ^{13}C and ^{12}C in marine waters vary by photosynthesis, deposition of organic matter, weathering rates, and submarine volcanism (Kump and Arthur 1999; Saltzman and Thomas 2014). Marine algae concentrate ^{12}C in organic matter thereby increasing $\delta^{13}C$ in ocean water and in carbonate minerals. The resulting sediments are black shale depleted in ^{13}C and limestone depleted in ^{12}C. The carbon isotope amount is affected by a complex set of interacting factors (Leckie et al. 2002; Saltzman and Thomas 2014) and during the Cretaceous fluctuated greatly (Veizer et al. 1999) even as the amount of modeled atmosphere CO_2 declined (Berner and Kothavala 1999).

Several challenges emerge with the use of geochemical signals as chronostratigraphic markers. First is that the shape and precision of the curves are related to sample density. The sample spacing varies depending on the rate of sediment accumulation; closer spacing is required in thinner intervals deposited at slower rates. A second issue is unraveling the effects of diagenesis from the original deposition signal. Verifying that an original depositional signal is recorded is based on multiple analyses, which have been clearly outlined by various authors (Menegatti et al. 1998; Bralower et al. 1999; Wendler et al. 2009; Jenkyns 2010; Wendler 2013). A third challenge is to define consistently and objectively the segment boundaries in the curve. Many geochemical curves are asymmetric and the curve trends are irregular and of different magnitudes; some curve shifts are abrupt and some are gradual. Placement of a boundary may be at the acme or the nadir, or at the beginning or ending or mid-point of the inflection, or part way along a gradually declining slope. A fourth challenge in using chemostratigraphic curves as chronostratigraphic markers is the lack of uniqueness of curve segments, so the segments must be integrated with precise biostratigraphic or magnetostratigraphic events. However carbon and oxygen isotope curves of strata younger than about 5 Ma seem to have distinctive characteristics that represent the 400 kyr eccentricity orbital cycles (Berggren and Burckle 1997; Wang et al. 2010).

These issues have been well addressed by studies of numerous Cretaceous Tethyan hemipelagic sections (text-fig. 1), in which the carbon isotope signal of bulk carbonate and of organic matter have been subdivided into discrete segments. Eight carbon isotope segments were initially defined in the Roter Sattel section, Switzerland, and the Cismon core, Italy (Menegatti et al. 1998). Subsequently segments C9 to C15 were defined in the upper Aptian-lower Albian pelagic section in Santa Rosa Canyon, Mexico (Bralower et al. 1999) (text-fig. 1). These segments are identified here in the high-resolution isotope curve of the core on Resolution Guyot (Jenkyns 1995; Jenkyns and Wilson 1999). Barremian carbon isotope segments B1-8 were first defined in the Cismon core and correlated with sections in the Swiss Alps, which were based on bulk rock samples of carbonate ramp limestone and marl (Wissler et al. 2002).

Subsequently carbon isotope segments were defined in a composite set of carbonate sections in southeastern France (Huck et al. 2013; 2014) and offshore Morocco in DSDP 545, which were given a different nomenclature (Herrle et al. 2004). The segments of Herrle et al. (2004) have been identified in Sonora (Madhavaraju et al. 2013). In the Pyrenees of Spain Barremian-Aptian segments are also described (Sanchez-Hernandez, Y. and Maurrasse 2014a, 2014b). Further examination of carbon isotope increment C7 resulted in dividing it into four subunits (Nuñez-Useche et al. 2014).

Upon shallow-water Tethyan carbonate platforms in the Mediterranean area, Barremian-Albian metric-scale shoaling-up cycles are defined by exposure contacts (d'Argenio et al. 2004; Wissler et al. 2004). Cyclostratigraphic analysis of lithostratigraphic cycles relates these to ~400 kyr-long eccentricity frequency. The carbon isotope signal in these platform sections is correlative with pelagic curves where constrained by magnetostratigraphic and biostratigraphic data.

The first purpose of this note is to calibrate numerical ages of Barremian-Albian carbon isotope segments defined by Menegatti et al. (1998), Bralower et al. (1999) and Wissler et al. (2002) and to integrate these segments with other biostratigraphic events. The integration of carbon isotope segments with biostratigraphic events in CRETCSDB4 (Scott 2014) has the potential to correlate stage boundaries of reference sections with signals in other sections. Second, precise numerical ages of Barremian-Albian carbon isotope segments will provide rates of change of processes that altered the oceanic carbon cycle.

METHOD OF INTEGRATION

The Cretaceous Chronostratigraphic Database CRETCSDB4 was constructed by graphic correlation, which is a transparent, testable method that integrates stratigraphic data. Graphic correlation is a quantitative but non-statistical technique that enables stratigraphic correlation experiments between two sections by comparing the ranges of event records in both sections (Edwards 1989; Carney and Pierce 1995). A graph of any pair of sections is an X/Y plot of the FOs (first appearances) and LOs (last appearances) of taxa found in both sections. To propose coeval relationships between sections, the interpreter places a line of correlation (LOC) through the tops and bases that are at their maximum range in both sections. This LOC is the most constrained hypothesis of synchroneity between the two sections and adjusts the ranges of the fewest bioevents. The LOC also accounts for hiatuses or faults at stratal discontinuities indicated by the lithostratigraphic record. The position of the LOC is defined by the equation for a regression line. Carney and Pierce (1995) explained the process and provided examples of the graphic technique.

A species range database such as CRETCSDB4 is compiled by iteratively graphing successive measured sections or cores and integrating ranges of all sections. Because the software GraphCor, a DOS-based system, has a limited storage capacity, sets of sections are grouped into subprojects of up to fifty sections of composited ranges that are then saved separate databases. The progressive subprojects that compose CRETCSDB4 are MIDK3, MIDK4, MIDK 41, MIDK45, CRET1, CRET2, and CRETFIX (Scott 2014). If a section in a preceding subproject is plotted to the next project, the plot will be a straight line because the data of the section is already in the composited dataset. The accuracy of these ranges depends on

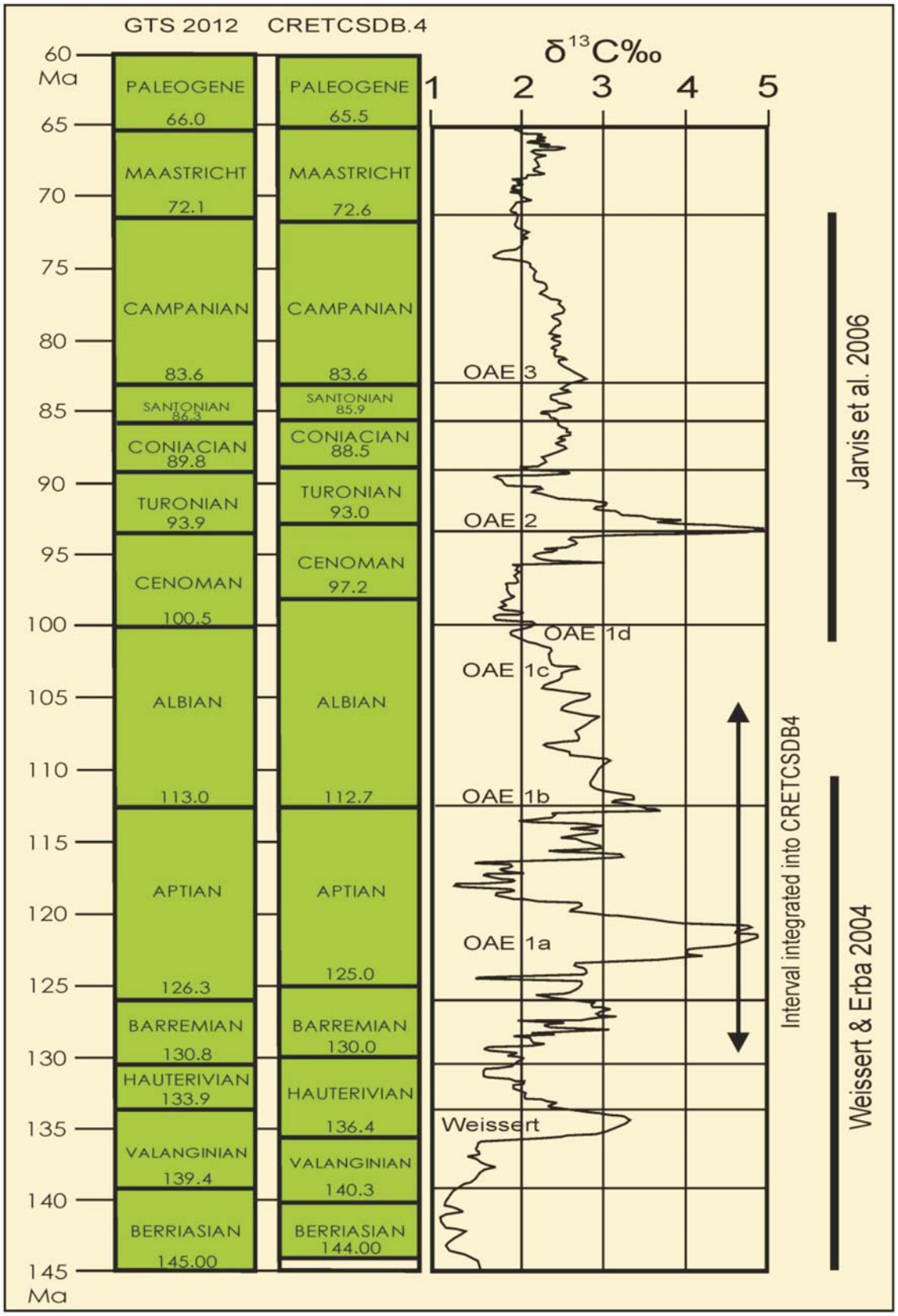

TEXT-FIGURE 1
Cretaceous geologic time scale calibrated by Gradstein et al. (2012) and Scott (2014) with composited carbon isotope curve of Weissert and Erba (2004), Jarvis et al. (2006) as presented by Steuber et al. (2015). Anoxic segments from Jenkyns (2010). Ma = megaannums. OAE = oceanic anoxic event.

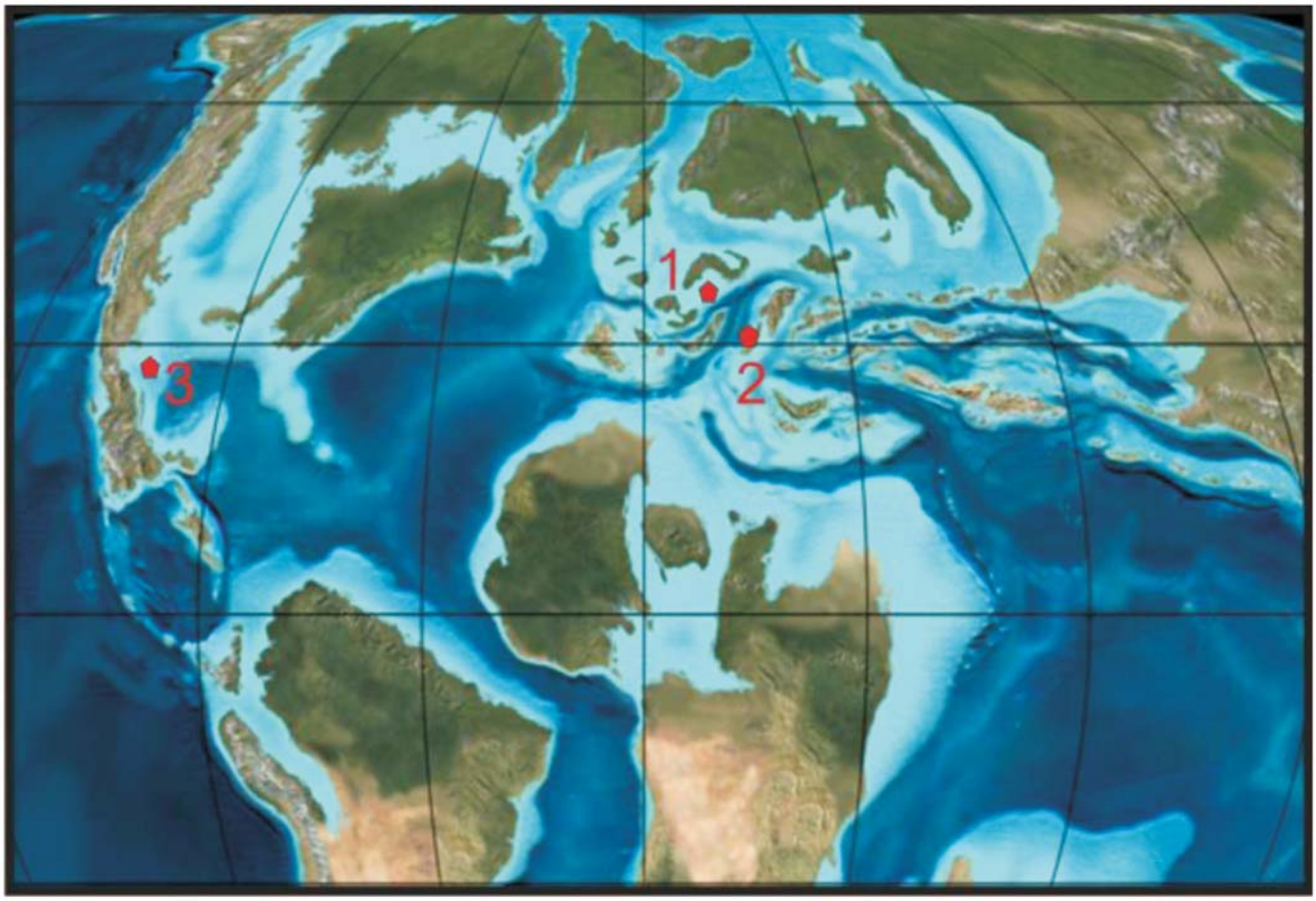

TEXT-FIGURE 2
Cretaceous paleogeography about 90 Ma as Mollweide projection showing relative locations of the Roter Sattel section (1), the Cismon core (2) and the Santa Rosa Canyon section (3) (red pentagon symbols). From Dr. Ron Blakey website: <http://jan.ucc.nau.edu/~rcb7/>.

the number of sections, preservation and correct identification of the species. Event sequences and ages compiled by graphic correlation can be tested and fully evaluated because the sources of the data are available. In addition, the order of segments in different basins can be compared.

CRETCSDB4 is a compilation of more than 3500 taxa and marker beds in more than 295 published sections calibrated to a mega-annum scale (Scott 2014). The database spans the Jurassic/Cretaceous and the Cretaceous/Paleogene boundaries. Construction of CRETCSDB4 began by plotting bioevents in the Kalaat Senan, Tunisia, Cenomanian-Turonian section to the 1989 time scale (Harland et al. 1990), which was subsequently adjusted to the 2004 time scale (Gradstein et al. 2004, 2012). The sedimentology, sequence stratigraphy, and biostratigraphy of the Kalaat Senan section were precisely documented and stage boundaries defined biostratigraphically (Robaszynski et al. 1993). Non-biotic data such as chemostratigraphic curves and sequence boundaries were incorporated into the database by including these segments with associated fossils in key reference sections (Edwards 1989). Groups of sections were combined into the database in successive subprojects, including the MIDK3, MIDK4, MIDK41, MIDK45, CRET1, and CRET2 databases that combine to compose CRETCSDB4. Additional sections with radiometrically dated beds were graphed to constrain the accuracy of the numerical scale. Ranges of first and last occurrences are calibrated to mega-annums of Cretaceous stages defined by GSSPs or reference sections. This database serves as a look-up table for interpolation and age calibration of other stratigraphic sections. The age ranges of some taxa and marker beds are preliminary and may be extended as new sections are added to the database.

CARBON ISOTOPE SECTION DATA

Barremian-Aptian carbon isotope segments were first identified in three Aptian basinal hemipelagic sections; two are in a rifted basin on the European side of the Tethys Ocean, at Cismon, Italy and Roter Sattel, Switzerland, and one section is in the Gulf of Mexico at Santa Rosa Canyon, Mexico (text-fig. 2; Appendix 1). Planktic foraminifera and nannoplankton are well preserved in each section and provide biostratigraphic control. The Cismon 120m-thick cored section is in the Venetian Alps of Northern Italy (Erba and Larson 1998; Erba et al. 1999; Wissler et al. 2002; Channell et al. 1979; 2000); a nearby outcrop section confirms the biostratigraphy (Bralower 1987). Magnetochrons M3r to M0r are identified in the Cismon cored section. The Roter Sattel section is in the Swiss Préalpes Médianes Plastiques and a

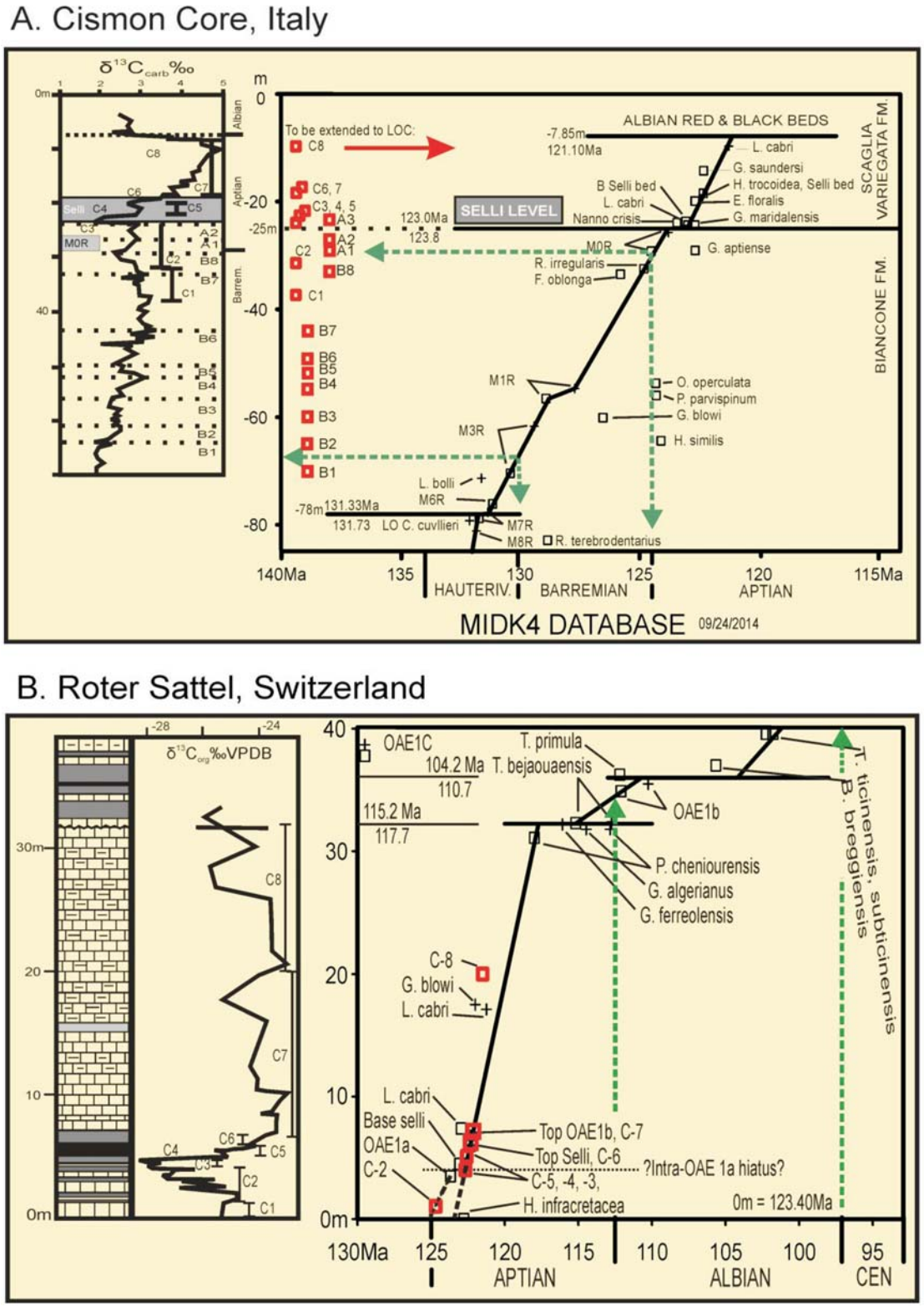

TEXT-FIGURE 3

Graphic plots of Cismon core (A) and Roter Sattel section (B) compared to the Cretaceous composited database. Square symbols = first occurrence or base of event; + = last occurrence or top of event; bases of geochemical segments are red squares; B1-6 and C1-8 are the bases of geochemical segments. A. Cismon core with line of correlation constrained by magnetochrons and Aptian bioevents. A slight disconformity or condensed interval is present at -25m at the base of the Livello Selli black shale. This plot first projects geochemical segments B-1-8 and C-1-8 into the numerical database; isotope curve from Erba et al. (1999) and Wissler et al. (2002, 2003). B. Roter Sattel outcrop section with line of correlation of Aptian interval constrained by OAE 1a and Selli bed. Base of C8 is above correlation line and LO of Leupoldina cabri by 2.9m, which is 2.18m higher than in Cismon core, which suggests that the boundary may be placed too high at Roter Sattel. At base of section C2 segment may define alternative LOC.

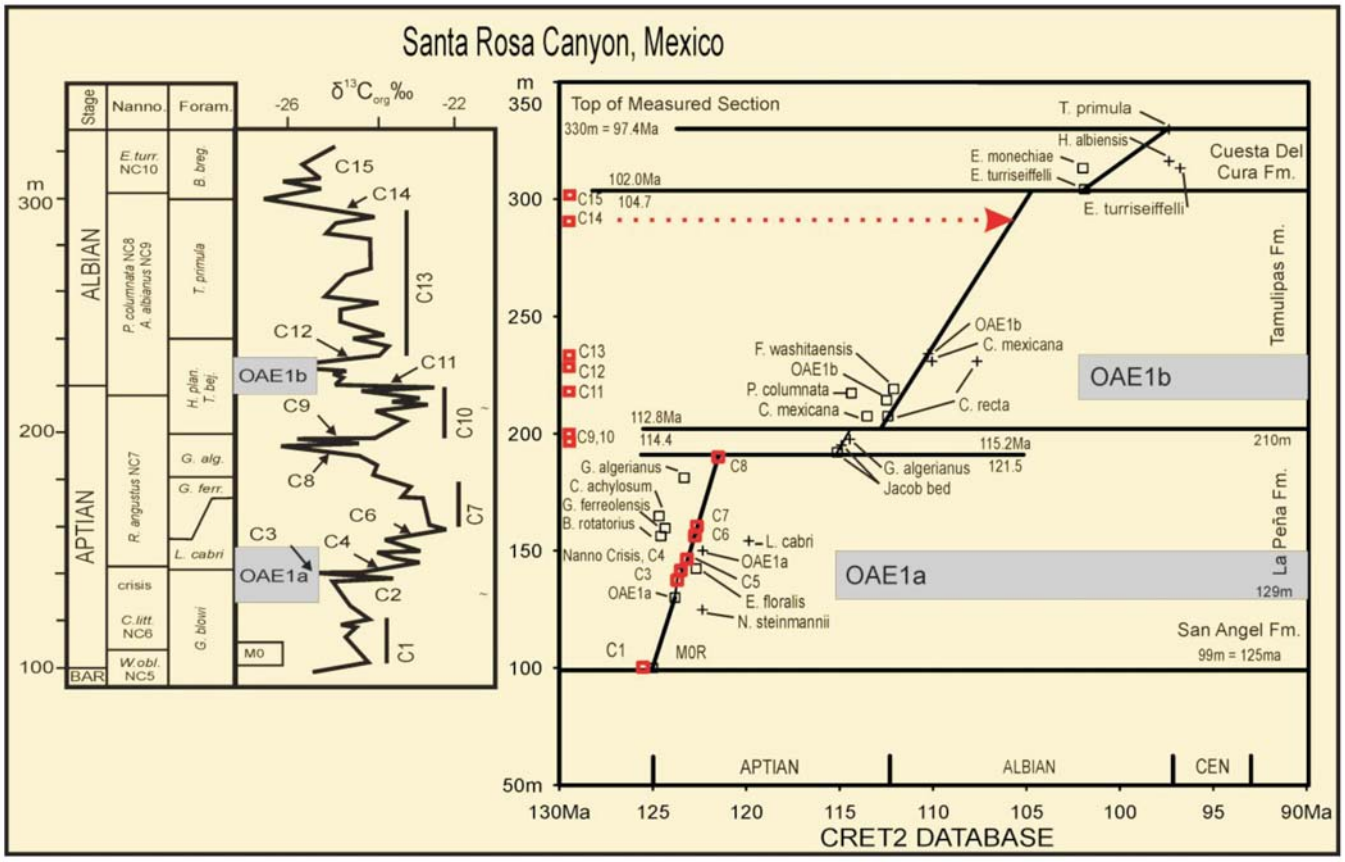

TEXT-FIGURE 4
Graphic plot of Santa Rosa Canyon section compared to the Cretaceous composited database (Symbols as in text-figure 3). Santa Rosa Canyon Aptian section line of correlation constrained by magnetochron M0R, OAE 1a and carbon segments set at Cismon and Roter Sattel. Numerical ages of Carbon isotope segments 9 through 15 calibrated to numerical ages by projecting metric position (red arrow) into upper Aptian-Albian interval by correlation line constrained by Niveau Jacob black shale, OAE 1b and bioevents.

bed-by-bed description documents the foraminifers and carbonate carbon isotope (Strasser et al. 2001). The Aptian-Albian interval is about 38m thick. The Santa Rosa Canyon outcrop section, Nuevo Leon, Mexico, is in the Sierra Madre Oriental and is 220m thick spanning basal Aptian to lower Albian.

At the Cismon cored section, bulk carbonate and organic carbon isotopes were measured on samples at a spacing of six to seven per meter (text-fig. 3A). These were divided into eight Aptian and five Barremian segments based on mean $\delta^{13}C_{carb}$ and $\delta^{13}C_{org}$ values (Menegatti et al. 1998; Erba et al. 1999; Wissler et al. 2002). Subsequently Wissler et al. (2003) further divided the upper Barremian and basal Aptian at Cismon into segments B6 to B8 and A1 to A4; segments B8 through A4 overlap segments C2 to C4 of Menegatti et al. (1998). The maximum differences in the curve are up to 3.8‰; some changes are abrupt and some gradational and boundaries are close to the inflections points of the shifts (Menegatti et al. 1998, figs. 2, 3; Erba et al. 1999, fig. 7). The Cismon section was plotted to the MIDK4 project, which is an early substage of CRECSDB4 (text-fig. 3A). The line of correlation is defined by magnetochrons, nannofossils and planktic foraminifera. The numerical ages of the bases of B1 to B8 and C to C8 were first projected into the database by this LOC.

Carbonate carbon isotope data in the Rotter Sattel section (text-fig. 3B) were derived from a spacing of six samples per meter (Menegatti et al. 1998, fig. 2). Some boundaries are very abrupt and others are at slopes between peaks. Planktic foraminifer biostratigraphy constrained the positions of the LOC. The boundaries of the $\delta^{13}C_{carb}$ and $\delta^{13}C_{org}$ curve segments plot on the LOC consistently as defined in the Cismon section. The base of C1 was not included because the section was not logged below the event base. C8 is left of the LOC and is higher in the section compared to its position and age in Cismon section; this suggests that its base was picked at different points on the curves in the two sections. The C7— C8 boundary in the Roter Sattel section is more gradational than in the Cismon section.

In the Roter Sattel section the Aptian-Albian unconformity at 32.25m is slightly above the base of C8 and no higher segments were noted by Menegatti et al. (1998, fig. 2). The graphic plot to the subproject MIDK41 of CRETCSDB4 suggests either a brief hiatus at the base of OAE 1a between C2 and C3 or a condensed interval (text-fig. 3B). An Aptian/Albian unconformity in both the Roter Sattel and Cismon sections limits the sequence of geochemical segments.

In the Santa Rosa Canyon section, Nuevo Leon, Mexico (text-fig. 4), samples were collected one meter apart and the or-

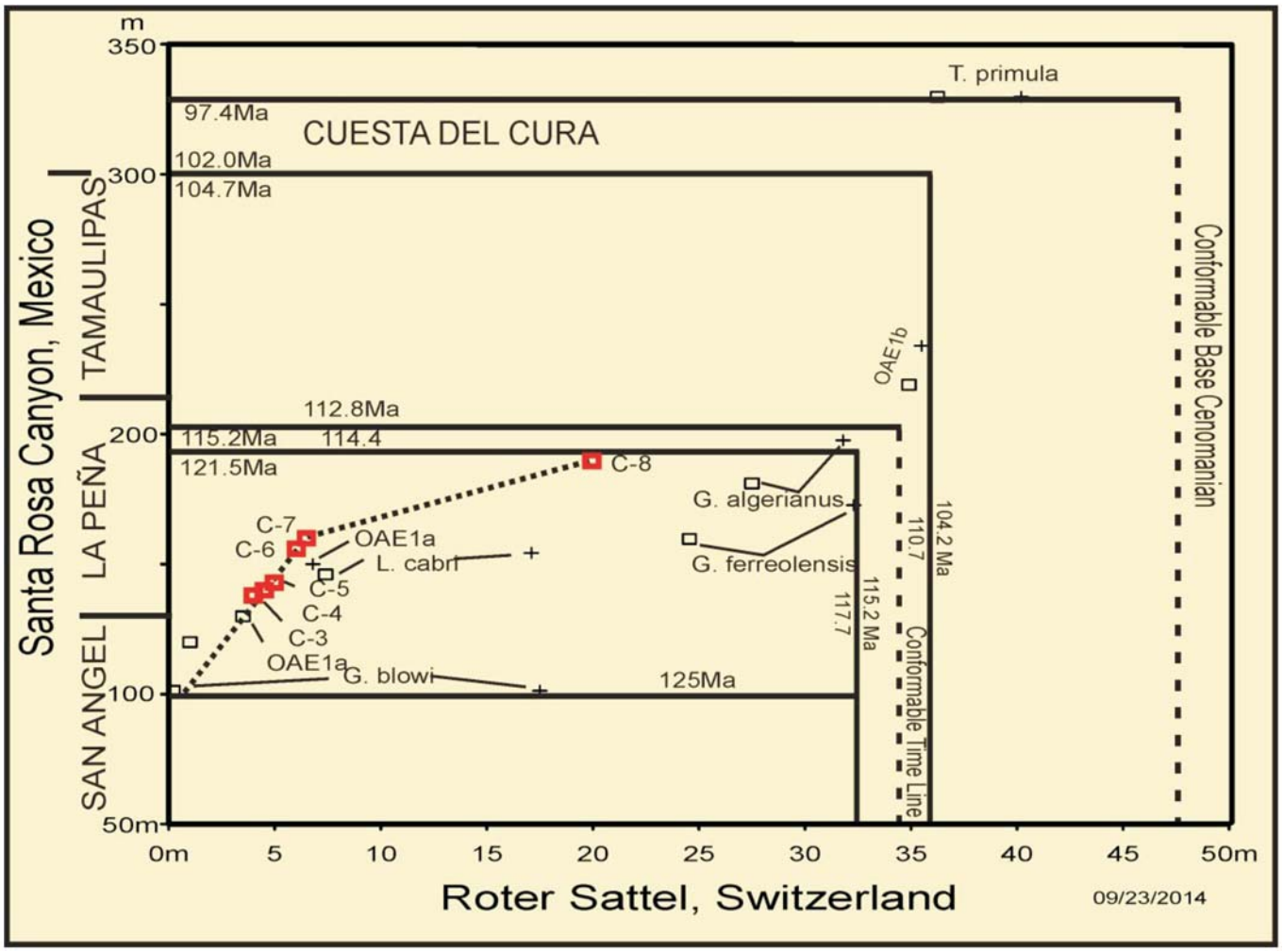

TEXT-FIGURE 5
Event ranges in Santa Rosa Canyon section compared to event ranges in Roter Sattel section showing that these segments are the same age in both sections. Line of correlation in Aptian interval is constrained by carbon isotope segments. Symbols as in text-figure 3. Unconformities (solid lines) are similar ages and conformable time lines (dashed lines) in Roter Sattel correlate with unconformities in Santa Rosa section.

ganic carbon of carbonate was measured. The total organic carbon content of the samples was generally less than 0.5%. The $\delta^{13}C_{org}$ values extend across unconformities into the Upper Albian *Eiffellithus turriseiffellii* and *Biticinella breggiensis* zones; bulk carbonate was not analyzed (Bralower et al. 1999, fig. 7). In addition to identifying C1 through C8, younger carbon segments C9 through C15 were defined. The boundary positions of the segments are on the inflection slopes between peaks or on the peaks themselves. Some segments correspond to peaks of total organic carbon and of $CaCO_3$%. Because curve segments are not unique, biostratigraphy was used to identify the older carbon segments. Nannofossil biostratigraphy (Bralower et al. 1999, fig. 3) was supplemented by planktic foraminifera, calpionellids and nannoconids (Longoria 1974, 1998; Ice and McNulty 1980; Sliter 1992). The chronostratigraphic interpretation of the section is constrained by magnetochron M0R at the base and the normal succession of nannofossil and planktic foraminifer zones up to basal Upper Albian (text-fig. 4).

The graphic plot of the Santa Rosa data to the Cretaceous Chronostratigraphic database (text-fig. 4) suggests discontinuities in the record of deposition based on offsets in the lines of correlation. These unconformities or condensed intervals had not been identified in Santa Rosa section previously. In the upper part of the La Peña Formation an unconformity is postulated at about 192m in the *Globigerinelloides algerianus* Zone above the base of segment C8, which is dated at 122.12 Ma. This level is the base of a 2‰ negative $\delta^{13}C_{org}$ shift and a 2.5% TOC peak, which is inferred to be the Niveau Jacob black shale bed projected at 115.13 Ma. This organic-rich bed is overlain by the Tamaulipas Limestone with OAE 1b in its basal part dated at 112.09 Ma. A second unconformity or condensed interval is proposed in the uppermost part of the La Peña at 210m between the LO of *G. algerianus* and the FO of *Colomiella recta*. Segments C9 and C10 are within this interval, which determines the projected age of these carbon isotope shifts. A higher unconformity at about 300m is between the Tamulipas and Cuesta Del Cura formations at a thin shale bed that overlies base of segment C15 and underlies the first occurrences

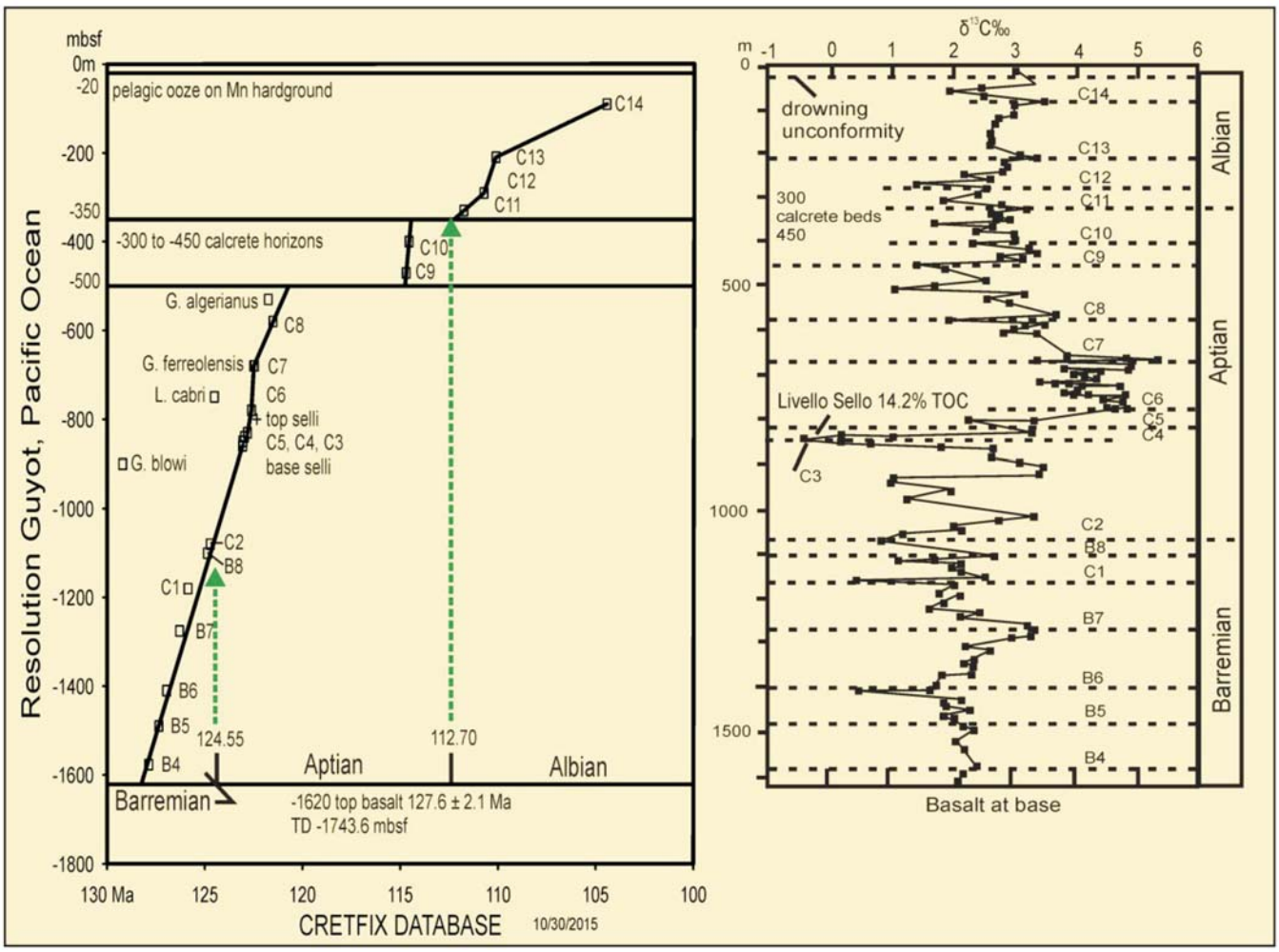

TEXT-FIGURE 6
Graphic plot of Resolution Guyot carbon isotope data relative to events in the advanced CRETFIX Database with the FOs positions of four planktic foraminifera projected by their relative positions with isotope events in the Cismon section by Jenkyns (1995). The base of the Aptian defined by the base of magnetochron M0R is at the base of carbon segment B8/C2 at -1100/-1080 mbsf. The base of the Albian as defined here by the FO of *Leymeriella tardefurcata* falls between the FOs of C10 and C11 -400 to -330 mbsf. Planktic foraminifers were not identified in the shallow shelf facies.

of Upper Albian *Eiffelithus turriseiffelii* and *Biticinella breggiensis*. The hiatus at this unconformity was correlated with a regional unconformity on the shelf interior of North Texas between the Fredericksburg and Washita groups Albian sequence boundary Al Wa 1 (Scott et al. 1988, fig. 4; Scott et al. 2003).

The carbon segments in the Aptian portion of the Santa Rosa section correlate well with those in the Roter Sattel section (text-fig. 5). In both sections an unconformity is plotted above the base of C8, although deposition persisted longer during event C8 at Roter Sattel than at Santa Rosa. This plot supports the correlation of Aptian carbon curve segments at Santa Rosa with those at Roter Sattel.

The Albian carbon isotope data is quite complex and not readily subdivided into unique segments. A rich dataset of deep benthic foraminifers from five different basins has a 4‰ spread of $\delta^{13}C$ without distinct segments (Friedrich et al. 2014, fig. 2). Furthermore, in the Albian Marne a Fucoid Formation at Mont Petrano, Italy, the amplitude of the cycles diminishes from about 0.75 ppm to 0.4 ppm (Giorgioni et al. 2014). These datasets suggest that oceanic processes shifted during the Albian (Giorgioni et al. 2014; Friedrich et al. 2014).

In order to test the correlation potential of Albian carbon isotope segments C9 to C14 the high resolution carbon isotope dataset of the Resolution Guyot core (Jenkyns 1995; Jenkyns and Wilson 1999) was graphed with the data at Santa Rosa Canyon in the CRETFIX database (text-fig. 6). This Mid-Pacific section spans a nearly 1600m-thick Barremian-Albian interval. This subtidal-intertidal carbonate section was deposited upon a basaltic edifice dated at 127.6±2.1 Ma (Jenkyns 1995) and re-calibrated to 123.63±0.9 Ma (Pringle in Larson and Erba 1999) so the oldest carbonate deposition was early Barremian, which began about 130 Ma (Ogg et al. 2012; Scott 2014). Supplementary chronostratigraphic control is limited in this section. The Selli marker bed was identified as a sixty meter thick interval of cyclic packstone-wackestone and algal laminite with clay and organic-rich laminae from 860m to 800m and a strongly negative carbon isotope peak (Jenkyns 1995) identified here as C3. The

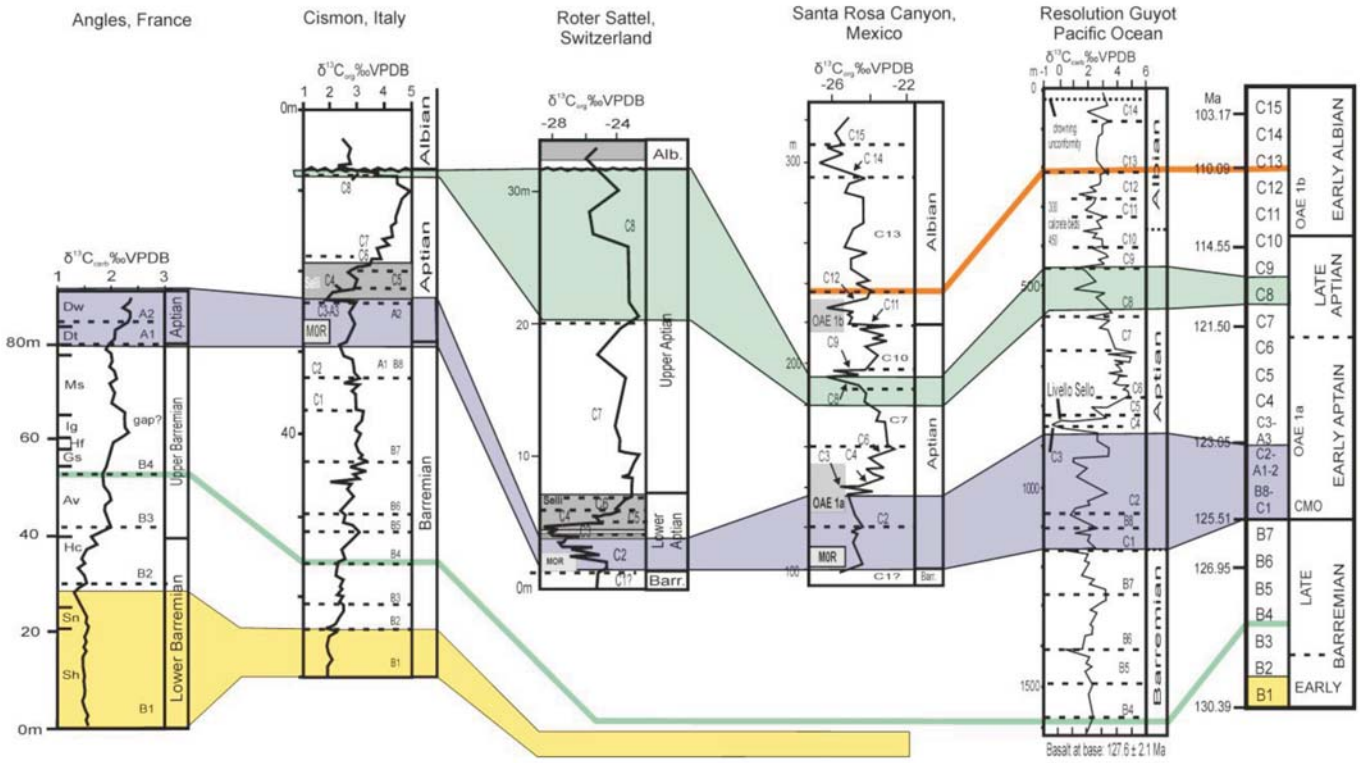

TEXT-FIGURE 7
Chemostratigraphic correlation of five key Tethyan carbonate sections that span the Barremian to Albian stages and that define the chronostratigraphic order of Carbon Isotope segments B1 to C15. Data for the Angles section from Wissler et al. (2002); for the Cismon section from Erba et al. (1999, fig. 7) and Menegatti et al. (1998, figs. 2, 3); for the Roter Sattel section from (Strasser et al. 2001; Menegatti et al. (1998, figs. 2, 3); and for the Santa Rosa section from Bralower et al. (1999, figs. 3, 7). Ammonite zonation of the Angles section is by Wissler et al. (2009): Av=*Ancycloceras vandenheckei*; Dt=*Deshayesites tuarkyricus*; Dw=*Deshayesites weissi*; Gs=*Gerhardtia sartousiana*; Hc=*Holcodiscus caillaudianus*; Hf=*Hemihoplites feraudianus*; Ig=*Imerites giraudi*; Kn=*Kotetishvilia nicklesi*; Ms=*Martelites sarasini*; Sh= *Spitidiscus hugii [*=Th=*Taveraidiscus hugii]*; Sn=*Subpuchellia nicklesi*; Tv=*Toxancyloceras vandenheckii*.

first occurrences of key Aptian planktic foraminifera were projected into the section by relating them to carbon isotope peaks in sections where the fossils are present (Larson and Erba 1999). Direct paleontological evidence of the Aptian age of the Resolution carbonates is the presence of the rudist bivalve, C*onchemipora skeltoni* Chartrousse and Masse (1998) at 917.0 mbsf. In the absence of other fossil data in the core, the Albian/Aptian boundary was approximated by $^{87}Sr/^{86}Sr$ curve (Jenkyns and Wilson 1999, fig. 5).

Identification of the carbon isotope segments defined in the Mediterranean and Mexican sections (text-fig. 6) is derived by comparing the curve parts below and above the strong negative peak C3. The first trial to identify lower Aptian-Barremian segments below C3 was to assume that basal Barremian B1 was the basal segment and segments were partitioned up to C3. However, the interval below C3 is too thin to accommodate segments B6-8. The second trial was to identify segments downward from C3 ending with B4 at the base. This resulted in a graphic interpretation (text-fig. 6) that projects the Barremian-Aptian contact near the base of C2 at about 930m. Carbon isotope segments above C3 match the placement of the segments in the Santa Rosa section up to C14, which on Resolution Guyot is truncated by a drowning unconformity marked by a manganese hardground. Within the interval 450 to 300m calcrete contacts are numerous and the carbon isotopes segments are thin, which is consistent with numerous brief hiatuses of subaerial exposure.

Wissler et al. (2002) first defined Barremian segments in the Cismon core data of Erba et al. (1999) and in the Angles, France section. The B1 to B5 and A1 to A4 segments were projected into the CRETCSDB4 by graphing these sections (text-fig. 3B). Subsequently Barremian-lower Aptian carbon isotope data were documented in two Swiss outcrop sections, Alvier and Churfirsten. Carbon isotope data were measured on bulk samples of limestone and marl (Wissler et al. 2003). The Barremian-lower Aptian interval at Alvier is about 440m thick and the Churfirsten section is 200m thick; at both sections sample spacing was about 2m. These two Swiss carbonate sections are bounded by a basal transgressive disconformity with Hauterivian-lower Barremian ammonites and by Upper Aptian ammonites above the topmost disconformity. The inclusion of these two sections confirmed the age interpolation of these isotope curves and their plots are not illustrated.

INTEGRATION WITH BIOEVENTS AND MAGNETOCHRONS

Foraminiferal zones are documented in two of the three key Aptian sections based on the first occurrance datum (FO) (Table 1). Segments C1 through C6 are within the *Globigerinelloides*

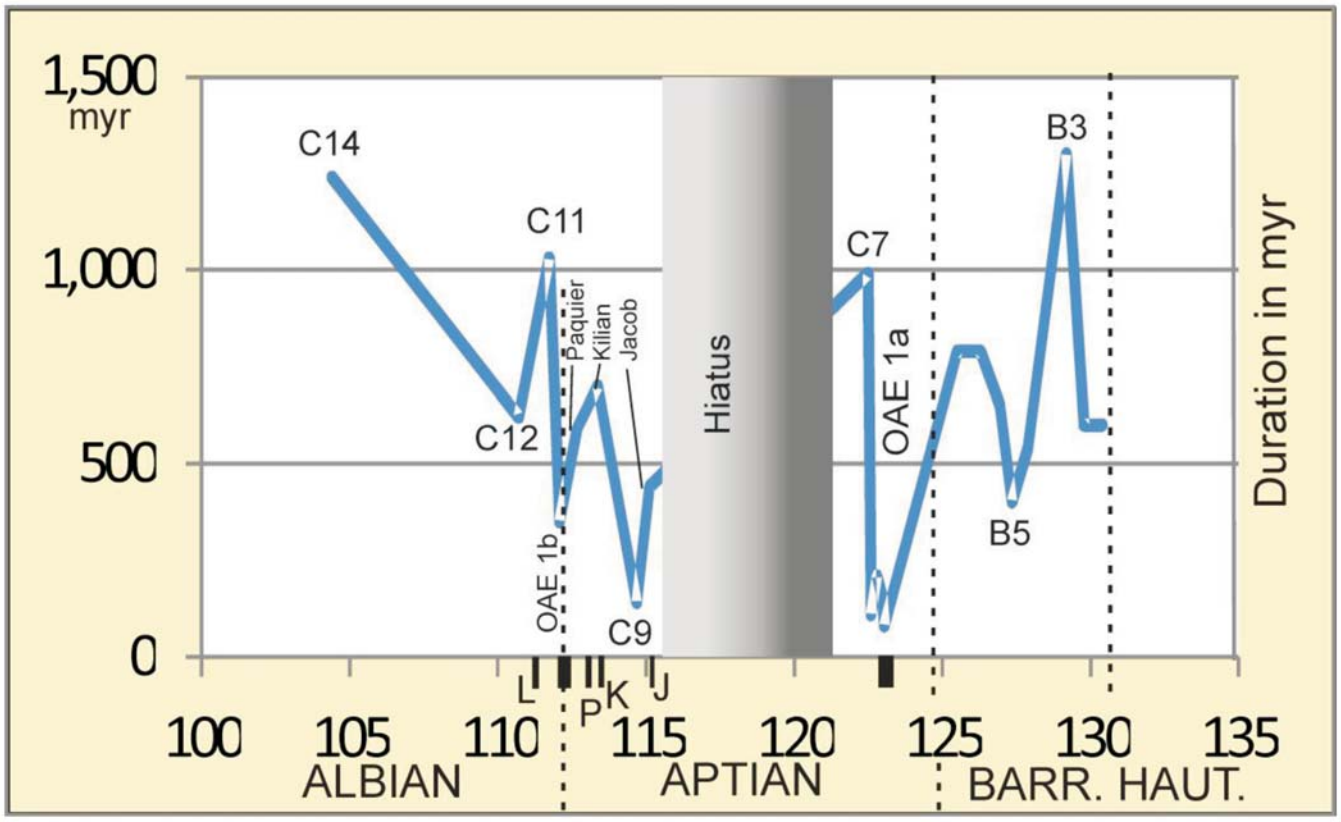

TEXT-FIGURE 8
Plot of carbon isotope segment durations versus time in mega-annums based on Table 1. Segments below unconformities and Wissler segments B8, A1, A2, and A3 that overlap C1, C2 segments are not included. Barremian durations fluctuate decreasing into OAE 1a, which is followed by a long period C7. Complete segment C8 is not shown because it is cut by a regional unconformity. Upper Aptian carbon isotope segment fluctuate decreasing into OAE 1b, which is followed by long segments C11 and C14. Leenhardt and Urbino black shale beds were deposited during isotope segment C11 and C12.

blowi Zone at the base of the Cismon and Rotter Sattel sections. The base of C7 is just below the base of the *Leupoldia cabri* Zone and ranges to the top of this zone. Segment C8 extends through the overlying *Globigerinelloides ferreolensis* and *Globigerinelloides algerianus* zones at Roter Sattel and is overlain by the Aptian-Albian unconformity in both sections (Menegatti et al. 1998; Strasser et al. 2001). At Santa Rosa thin C9 is in the uppermost part of the *Globigerinelloides algerianus* Zone and C10 begins in the *Hedberella planispira-Ticinella bejaouaensis* Zone and C11-12 span to the top of this zone. C13 and C14 span the *Ticinella primula* Zone. A disconformity separates C14 from C15, which spans part of the *Biticinella breggiensis* Zone.

Nannofossil zones are documented in the Cismon core and the Santa Rosa outcrop. Segment C1 begins in the lower part of the *Chiastozygus litterarius* Zone NC6 identified by the first occurrence (FO) of *Rucinolithus irregularis* (Bralower et al. 1999) (Table 1). Segments C4 through C10 range through the *Ragodiscus angustus* Zone NC7 identified at Santa Rosa Canyon by the FO of *Eprolithus floralis*. Segments C11 through C14 are within the *Prediscosphaera columnata* Zone NC8 and the *Axopodorhabdus albianus* Zone NC9, which are undifferentiated at Santa Rosa Canyon.

In the Cismon cored section magnetochrons M0R to M9R (Erba et al. 1999) are integrated with nannofossils and carbon isotope segments (Menegatti et al. 1998). Segment C1 corresponds with Chron CM1R and C2 overlaps with Chron CM0R (text-fig. 2). However in the Santa Rosa Canyon section C1 extends across CM0R and C2 is younger beginning above CM0R. A comparison of the carbon isotope curves by Menegatti et al. (1998, fig. 3) with curves by Erba et al. (1999, fig. 7) and by Bralower et al. (1999, fig. 7) indicate that the base of C2 is defined at different places on the curves.

The base of carbon segment C3 is slightly younger than the onset of the nannoconid crisis and the base of C5 is virtually the same age as the beginning of OAE 1a in these sections (Table 1). In the younger part of the late Aptian-early Albian, carbon segments C9 to C12 in Santa Rosa section correlate in part with black shale beds defined in Italian sections although the beginning ages are not coincident.

No ammonites were recorded at the three sections but ammonite first occurrences can be correlated with the carbon isotope segments by the integration of ammonites from other sections that also yield nannofossils and planktic foraminifers (Table 1). The FO of the basal Aptian *Deshayesites oglanlensis* is in C2. The FO of *Epicheloniceras martini* in the Upper Aptian Substage is within C7. The lowermost Albian *Leymeriella tardefurcata* and *Leymeriella schrammeni schrammeni* dated at 112.46 Ma correlate within C10. One well preserved rudist specimen in the Res-

TABLE 1
Numerical ages of carbon isotope events compared to bioevent ages. The age of the base of a segment defines the age of the top of the preceding segment so the age of the top is redundant. Most last occurrences of taxa and magnetochrons do not constrain the line of correlation and most zones are defined by the FO, so only the ages of the FO of carbon segments are compared to FO of bioevents. Ages from CRETCSDB4 (Scott 2014; precisionstratigraphy.com).

Stages	Carbon Segments		Ma	Duration myr	Geochemical Markers Base	Ma	Ammonoidea FO	Ma	Planktic Foraminiferida FO	Ma	Calcareous Nannofossils FO	Ma
	C15		103.17									
	C14		104.41	1,240			*Mortoniceras pricei*	104.16				
							Dipoloceras cristatum	105.54			*Axopodorhabdus albianus*	108.81
	C13		110.09	5,680								
	C12		110.71	620	Niveau Urbino	110.66	*Leymeriella regularis*	110.94				
	C11		111.74	1,030	Niveau Leenhardt	111.21	*Douvilleiceras mammillatum*	111.58				
				350	OAE 1b	112.09						
				590	Niveau Paquier	112.68	*Leymeriella tardefurcata*	112.68	*Ticinella primula*	112.92		
				700	Niveau Kilian	113.38						
	Hiatus											
							Leymeriella schrammeni anterior	113.51	*Microhedbergella rischi*	113.61		
	C10		114.55	2,810							*Prediscosphaera columnata*	114.5
	C9		114.69	140			*Immunitoceras immunitum*	114.74				
				440	Niveau Jacob	115.13			*Paraticinella rohri*	115.46	*Hayesites albiensis*	115.19
	Hiatus											
	C8		121.5	6,810			*Aconeceras nisum*	121.94	*Ticinella bejaouaensis*	119.49	*Tranolithus orionatus*	120.81
	C7		122.49	990			*Epicheloniceras martini*	122.19				
	C6		122.6	110							*Rhagodiscus gallagheri*	122.63
	C5		122.81	210							*Eprolithus floralis*	122.71
APTIAN	C4		122.97	160			*Dufrenoyia furcata*	122.93				
	C3	A3	123.05	80	Selli bed	123.05			*Globigerinelloides algerianus*	123.07		
					Nannoconid Crisis	123.42	*Deshayesites inflatus*	123.44	*Leupoldina cabri*	123.14		
							Deshayesites deshayesi	123.61				
					OAE 1a	123.77	*Deshayesites weissi*	123.85				
	Hiatus											
	C2	A2	124.06	1,010								
		A1	124.33	270					*Globigerinelloides ferreolensis*	124.29		
		C2	124.72	390							*Rhagodiscus achlyostaurion*	124.67
		B8	124.86	140	M0R	125	*Deshayesites oglanlensis*	124.85				
	C1		125.51	650								
	B7		126.3	790								
	B6		126.95	650								
	B5		127.35	400			*Imerites [Colchidites] giraudi*	127.38				
	B4		127.89	540			*Gerharditia sartousiana*	128.2				
					M1R	128.91	*Toxancycloceras vandenhecki*	128.97				
							Kotetish. compressissima	129.71	*Globigerellinoides blowi*	129.2		
	B3		129.19	1,300			*Nicklesia pulchella*	129.72	*Hedberella kuznetsovae*	129.76		
	B2		129.79	600			*Kotetish. [Nickelsia] nicklesi*	129.91	*Hedbergella similis*	129.85		
	B1		130.39	600	M3R	130.44	*Taveraidiscus [Spitidiscus] hugii*	130.27				

olution core is the Aptian C*onchemipora skeltoni* at 917.0 mbsf (Chartrousse and Masse 1998) in the lower part of segment C2.

Because the carbon isotope segments are defined in hemipelagic basin sections, correlation of carbon segments with shelf sections where short-term hiatuses are numerous is uncertain (Quesne and Ferry 1995; Di Lucia et al. 2012). However, where shelf cycles are integrated with magnetochrons and OAEs, and carbon isotope curves are similar to nearby basin curves, there sea-level segments can be correlated with basin successions (d'Argenio et al. 2004; Wissler et al. 2004).

GLOBAL CORRELATION POTENTIAL

To be used as a chronostratigraphic tool carbon isotope curve segments must be related to independent criteria such as species FO or LO or magnetochrons; they must be consistently identified and represent segments of widespread oceanic changes. The carbon isotope datasets of five outcrop and cored sections in southern Europe, North America and the Pacific Ocean are integrated with independent chronostratigraphic markers and their curve shapes are relatively consistent and identifiable among the sections (text-fig. 7).

Lower Barremian strata at the Angles and Cismon sections conformably overlie Hauterivian sedimentary strata and span the *Taveraidiscus hugii* and *Kotestishvilia nicklesi* zones (Wissler et al. 2009). Carbon isotope event B1 spans these zones and the boundary with B2 is within Magnetocrhon CM3R at Cismon (Menegatti et al. 1998). The lower-upper Barremian boundary defined by the first occurrence of *Toxancycloceras vandenheckii* in the Angles and Cismon sections falls in the upper part of isotope event B2.

The Barremian-Aptian boundary can be consistently identified in all five sections. In the absence of a GSSP, this stage boundary is positioned approximately at the base of Magnetochron M0R and the first occurrence of the ammonite, *Deshayesites oglanlensis* or the alternative species at Angles, *Deshayesites tuarkyricus*. In the Cismon section the boundary is within carbon event C2 (Menegatti et al. 1998) and at the contact of B8 and A1 (Wissler et al. 2002, 2003). At Roter Sattel, Switzerland Menegatti et al. (1998) placed the base Aptian at the contact of C1 and C2. However, C1 was defined by four points at the base of the section so that no clear definition of the C1-C2 boundary is recorded. Also in the Santa Rosa, Mexico, section the basal data points were identified as C1 (Bralower et al. 1999) but could also be part of C2.

In the Lower Aptian, the sharp light carbon isotope peak C3 is the same age as the base of the Selli bed and slightly younger than the isotope inflection point used to define the beginning of OAE 1a. The closely spaced isotope segments C4-C6 are within OAE 1a. The positive peak used to define C7 approximates the end of the anoxic event.

Until a global section and stratal point is picked for the base of the Albian Stage, multiple criteria have been proposed: first occurrence of *Microhedbergella rischi/renilaevis* at 113.32 Ma, *Leymeriella schrammeni anterior* at 113.51 Ma and *Leymeriella tardefurcata* at 112.68 Ma (Petrizzo et al. 2012; Kennedy et al. 2014). These bioevents fall within carbon isotope event C10,

which spans 114.55-111.74 Ma. Carbon event C10 is a relatively positive interval bounded below and above by sharp light peaks in the Santa Rosa and Resolution Guyot sections. In the Cismon and Roter Sattel sections the Aptian-Albian boundary is an unconformity.

DURATIONS OF CARBON ISOTOPE SEGMENTS

The age calibration of carbon isotope segment bases measures the durations of the oceanic isotopic excursions (table 1, text-fig. 8). The age-duration plot shows fluctuating but gradually shorter carbon isotope segments leading to OAE 1a, which is followed by three very brief segments C4, 5, 6. This was followed by long C7 and C8, which was truncated by submarine unconformities in Cismon, Roter Sattel and Santa Rosa sections; the maximum duration of this hiatus was from 120 to 115.2 Ma. This hiatus was followed by short-term carbon burial segments represented by black shale beds Jacob, Kilian, Paquier, Leenhardt, and Urbino that clustered around OAE 1b. Long-period segments followed through the Early and Middle Albian Age. Changing durations of carbon isotope segments may be clues to changes in processes or the effects of the process that altered the ocean carbon reservoir. During the Barremian-Aptian interval, $\delta^{13}C$ spiked from 1 to 3.5‰ (Veizer et al. 1999, fig. 10), even as atmospheric CO_2 declined steeply (Berner and Kothavala 1999, fig. 13). Associated increased marine productivity and carbon burial suggest "widespread changes in the ocean-climate system" (Leckie et al. 2002). The very negative carbon isotope shift C3 is found in many Lower Aptian shelf-slope-basin sections. Aptian sea-floor spreading rates increased significantly (Seton et al. 2009). Beginning in Late Barremian crustal production increased by 44% from about 18 to 26 km^3/yr^{-1} and during early-middle Aptian production increased further 35% to 35 km^3/yr^{-1} (Leckie et al. 2002; Kelley 2003, fig. 7.16). Increased crustal production accounts for emplacement of the large igneous provinces (LIP) Ontong Java I-Mannihiki and Kerguelen I. Carbon isotope shifts in sedimentary strata may be related to one or more of three processes (Leckie et al. 2002): 1) increased upwelling of nutrient-rich and ^{12}C-rich waters (Menegatti et al. 1998); 2) increased weathering rates related to increased CO_2 and warmer atmosphere (Menegatti et al. 1998); and 3) injection of light mantle-derived CO_2 by LIP eruption followed by OAE 1a carbon burial (Larson and Erba 1999).

The mean duration of the twenty-one Barremian-early Albian segments is 587 kyr, which differs from the climatic cycle frequencies. However light and dark marl beds of the Selli Level in the Cismon core record eccentricity, (400 kyr), obliquity (36 kyr) and precession (20 kyr) (Huang et al. 2010). In the Central Apennines, Italy, carbon isotope of bulk carbonate of Albian marl records the 400 kyr cycle (Giorgioni et al. 2012). These authors conclude "that the cyclic pattern in the $\delta^{13}C$ curve reflects changes in the isotopic composition of the dissolved inorganic carbon in the photic zone of the Tethys during the Albian" (Giorgioni et al. 2012). These regular lithological cycles reflect the ocean-atmosphere climatic interaction. The irregular carbon isotope segments of the Barremian-early Albian may have responded to other processes such as submarine volcanic eruptions or changes in sea floor spreading rates or they could be divided more finely. The durations of the carbon isotope segments suggest that fractionation rates of light carbon from ^{13}C were abrupt.

CONCLUSIONS

Carbon isotope curve segments are integrated within the Cretaceous Chronostratigraphic Database by plots of the Roter Sattel, Cismon and Santa Rosa Canyon sections based on shared bioevents and magnetochrons. The bases of these carbon isotope segments acquire numerical ages by these correlations (table 1). These ages then are compared with the ages of the FOs of ammonites, planktic foraminifer and calcareous nannofossils that define the standard Aptian-Albian zones. Thus these geochemical records are correlated with criteria that define the suggested stage and substage boundaries (Reboulet et al. 2011), although no GSSPs have been yet ratified. The base of the Aptian as defined by Chron CM0R is within segment C1 or if the stage is defined by the FO of *Deshayesites oglanlensis* the base is in C2. If the base of the Upper Aptian Substage is defined by the FO of *Epicheloniceras martini*, the boundary is within C7. In 2000 the base of the Albian was defined by the FO of *Leymeriella tardefurcata* or *Leymeriella schrammeni schrammeni* (Kennedy et al. 2000) dated at 112.46 Ma, which is within C10. However new data from the pré-Guitard section in southern France places the base Albian at the first appearance of the planktic foraminifer *Microhedbergella renilaevis* Huber and Leckie 2011 (Kennedy et al. 2014), which is in the middle of Niveau Kilian. In CRETCSDB4 the FO of *M. renilaevis* is 113.29 Ma and Niveau Kilian is 113.36-113.24 Ma. The age of carbon isotope stage 10 is 114.55-111.74 Ma.

The durations of the oceanic isotopic segments are measured by the numerical age calibrations of the base of each carbon isotope event. The mean duration of 587 kyr is longer than the 400 kyr eccentricity cycle. The durations of the carbon isotope segments suggest that processes in addition to climate may have been a driver of these segments. It should be noted that the longer segments could likely be subdivided by further refinement of the carbon isotope curve with closer spaced samples. Increasing the number of segments could produce a cycle frequency nearer 400 kyr.

ACKNOWLEDGMENTS

The excellent, thorough data collected and published by numerous authors provided the data for this stratigraphic experiment. Research on the classic Mural Formation in Sonora by Jayagopal Madhavaraju and Carlos González-León, Estación Regional del Noroeste, Instituto de Geologica, Universidad Nacional Autónoma de México, Hermosillo, prompted this study. I appreciate the constructive reviews, which improved the manuscript, and especially the support and suggestions of Lucy Edwards.

REFERENCES

D'AREGENIO, B., FERRERI, V., WEISSERT, H., AMODIO, S., BUONOCUNTO, F. P. and WISSLER, L., 2004. Amultidisciplinary approach to global correlation and geochronology. The Cretaceous shallow-ater carbonates of southern Apennins, Italy. In: d'Argenio, B., Fischer, A. G., Premoli Silva, I., Weissert, H. and Ferreri, V., Eds., Cyclostratigraphy: Approaches and case histories. *SEPM Special Publication* No. 81: 103–122.

BERGGREN, W. A. and BURCKLE, L. H., Jr., 1997. The Pliocene-Pleistocene boundary in deep-sea sediments. In: Van Couvering, J. A., Ed., *The Pleistocene boundary & the beginning of the Quaternary*, 87–103. Cambridge University Press.

BERNER, R. A. and KOTHAVALA, Z., 1999. GEOCARB III: A revised model of atmosphere CO_2 over Phanerozoic time. *American Journal of Science*, 301: 182–204.

BRALOWER, T. J., 1987. Valanginian-Aptian calcareous nannofossil stratigraphy and correlation with the upper M-sequence magnetic anomalies. *Marine Micropaleontology* 11: 293–310.

BRALOWER, T. J., COBABE, E., CLEMENT, B., SLITER, W. V., OSBURN, C. L. and LONGORIA, J., 1999. The record of global change in mid-Cretaceous (Barremian-Albian) sections from the Sierra Madre, Northeastern Mexico. *Journal of Foraminiferal Research*, 29: 418–437.

BURLA, S., HEIMHOFER, U., HOCHULI, P. A., WEISSERT, H. and SKELTON, P., 2008. Changes in sedimentary patterns of coastal and deep-sea successions from the North Atlantic (Portugal) linked to Early Cretaceous environmental change. *Palaoegeography, Palaeoclimatology, Palaeoecology*, 257: 38–57.

CARNEY, J. L. and PIERCE, R. W., 1995. Graphic correlation & composite standard databases as tools for the exploration biostratigrapher. In: Mann K.O. and Lane H.R., Eds., *Graphic Correlation*, 23–43. SEPM (Society for Sedimentary Geology), Tulsa, Special Publication 53.

CHANNELL, J. E. T., LOWRIE, W. and MEDIZZA, F., 1979. Middle and Early Cretaceous magnetic stratigraphy from the Cismon section, Northern Italy. *Earth and Planetary Science Letters*, 42: 153–166.

CHANNELL, J. E. T., ERBA, E., MUTTONI, G. and TREMOLADA, F., 2000. Early Cretaceous magnetic stratigraphy in the APTCORE drill core and adjacent outcrop at Cismon (Southern Alps, Italy), and correlation to the proposed Barremian-Aptian boundary stratotype. *Geological Society of America Bulletin*, 112: 430–1443.

CHARTROUSSE, A. and MASSE, J.-P., 1998. Coalcomaninae (Rudistes, Caprinidae) nouveaux de L'Aptien Inférieur des Mid Pacific Mountains. *Geobios – Mémoire spécial* no. 22:87–92.

CLARKE, L. J. and JENKYNS, H. C., 1999. New oxygen-isotope evidence for long-term Cretaceous climate change in the southern hemisphere. *Geology*, 27: 699–702 doi:10.1130/0091-7613(1999)027<0699:NOIEFL>2.3.CO;2.

DI LUCIA, M., TRECALLI, A., MUTTI, M. and PARENTE, M., 2012. Bio-chemostratigraphy of the Barremian-Aptian shallow-water carbonates of the southern Apennines (Italy):pinpointing the OAE1a in a Tethyan carbonate platform. *Solid Earth*, 3:1–28, doi:10.5194/se-3-1-2012.

EDWARDS, L. E., 1989. Supplemented graphic correlation: A powerful tool for paleontologists and nonpaleontologists. *Palaios*, 4: 127–143.

ERBA, E. and LARSON, R. L., 1998. The Cismon APTICORE (Southern Alps, Italy): A "reference section" for the Lower Cretaceous at low latitudes. *Rivista Italiana di Paleontogia e Stratigrafia*, 104: 181–192.

ERBA, E., CHANNELL, J. E. T., CLAPS, M., JONES, C., LARSON, R., OPDYKE, B., PREMOLI SILVA, I., RIVA, A., SALVINI, G. and TORRICELLI, S., 1999. Southern Alps, Italy: A "reference section" for the Barremian-Aptian interval at low latitudes. *Journal of foraminiferal Research*, Washington D.C., vol. 29, p. 371–391.

ERBACHER, J., THUROW, J. and LITTKE, R., 1996. Evolution patterns of radiolaria and organic matter variations: A new approach to identify sea-level changes in mid-Cretaceous pelagic environments. *Geology*, 24: 499–502.

FRIEDRICH, O., NORRIS, R.D. and ERBACHER, J., 2012. Evolution of middle to Late Cretaceous oceans — A 55m.y. record of Earth's temperature and carbon cycle. *Geology*, 40: 107–110; doi: 10.1130/G32701.1.

FÖLLMI, K. B., GODET, A., BODIN, S. and LINDER, P. 2006. Interactions between environmental change and shallow water carbonate buildup along the northern Tethyan margin and their impact on the Early Cretaceous carbon isotope record. *Paleoceanography*, 21: PA4211, doi:10.1029/2006PA001313.

GAMACORTA, G., JENKYNS, H. C., RUSSO, F., TISKOS, H., WILSON, P. A., FAUCHER, G. and ERBA, E., 2015. Carbon- and oxygen-isotope records of mid-Cretaceous Tethyan pelagic sequences from the Umbria-March and Belluno Basins (Italy). *Newsletters on Stratigraphy*, 48: 299–323.

GIORGIONI, M., WEISSERT, H., BERNASCONI, S. M., HOCHULI, P. A., COCCIONI, R. and KELLER, C. E., 2012. Orbital control on carbon cycle and oceanography in the mid-Cretceous greenhouse. *Paleoceanography*, 27: PA1204, doi:10.1029/2011PA002163 .

GRADSTEIN, F., OGG, J. and SMITH, A., 2004. A geologic time scale 2004: *Cambridge University Press*, 589 p.

GRADSTEIN, F. M. OGG, J. G., SCHMITZ, M. D. and OGG, G., 2014. The Geologic Time Scale 2012. *Elsevier*, 2 vol., 1176 p.

HARLAND, W. B., ARMSTRONG, R. L., COX, A. V., CRAIG, L. E., SMITH, A. G. AND SMITH, D. G., 1990. A geologic time scale 1989: *Cambridge University Press*, 263 p.

HAY, W. W., 2009. Cretaceous oceans and ocean modeling. In: Hu, X., Wang, C., Scott, R. W., Wagreich, M. and Jansa, L., Eds., Cretaceous Oceanic Red Beds: Stratigraphy, Composition, Origins, and Paleogeographic and Paleoclimatic significance. *SEPM (Society for Sedimentary Geology)* Special Publication No. 91, 243–271.

HERRLE, J. O., KÖBLER, P., FRIEDRICH, O., ERLENKEUSER, H. and HEMLEBEN, C., 2004. High-resolution carbon isotope records of the Aptian to Lower Albian from SE France and the Mazagan Plateau (DSDP Site 545): a stratigraphic tool for paleoceanographic and paleobiologic reconstruction. *Earth and Planetary Science Letters*, 218: 149–161.

HU, X., SCOTT, R.W., CAI, Y., WANG, C. and MELINTE-DOBRINESCU, M.C. 2012. Cretaceous oceanic red beds (CORBs): Different time scales and models of origin. *Earth-Science Reviews*, 115:217–248.

HUANG, C., HINNOV, L., FISCHER, A. G., GRIPPO, A. and HERBERT, T., 2010. Astronomical tuning of the Aptian Stage from Italian reference sections. *Geology*, 38:899-902; doi: 10.1130/G31177.1.

HUCK, S., HEIMHOFER, U., IMMENHAUSER, A. and WEISSERT, H., 2013. Carbon-isotope stratigraphy of Early Cretaceous (Urgonian) shoal-water depsoits: Diachronous changes in carbonate-platform production in the north-western Tethys. *Sedimentary Geology*, 290: 157–174. Dx.doi.org/10.1016/j.sedgeo.2013.03.016.

HUCK, S., STEIN, M., IMMENHAUSER, A., SKELTON, P. W., CHRIST, N., FÖLLMI, K. and HEIMHOFER, U., 2014. Response of proto-Atlantic carbonate-platform ecosystems to OAE 1a-related stressors. *Sedimentary Geology*, 313: 15–31. dx.doi.org/10.1016/j.sedgeo.2014.08.003.

ICE, R. G. and MCNULTY, C. L., 1980. Foraminifers and calcispheres from the Cuesta del Cura and lower Agua Nueva(?) formations (Cretaceous) in east-central Mexico. *Transactions of the Gulf Coast Association of Geological Societies*, 30: 403–425.

JARVIS, I., GALE, A. S., JENKYNS, H. C. and PEARCE, M. A., 2006. Secular variation in Late Cretaceous carbon isotopes: a new ^{13}C carbonate reference curve for the Cenomanian-Campanian (99.6-70.6 Ma). *Geological Magazine*, 143: 561–608.

JENKYNS, H. C., 1995. 6. Carbon-isotope stratigraphy and paleoceanographic significance of the Lower Cretaceous shallow-water carbonates of Resolution Guyot, Mid-Pacific Mountains. In: Winterer E., Sager, W. W., Firth, J. V. and Sinton, J. M., Eds., *Proceedings of the Ocean Drilling Program, Scientific Results,* vol. 143: 99–104.

JENKYNS, H. C., 2010, Geochemistry of oceanic anoxic segments . *Geochemistry, Geophysics, Geosystems,* 11, Q03004. doi:10.1029/2009GC002788.

JENKYNS, H. C., GALE, A. S. and CORFIELD, R. M., 1994. Carbon- and oxygen isotope stratigraphy of the English Chalk and Italian Scaglia and its palaeoclimatic significance. *Geological Magazine*, 131: 1–34.

JENKYNS, H. C. and WILSON, P. A., 1999. Stratigraphy, paleoceanography, and evolution of Cretaceous Pacific guyots: Relics from a Greenhouse Earth: *American Journal of Science*: 299:341–392.

KELLEY, S. P., 2003. 7 Volcanic inputs. In: Skelton, P.W., Ed., The Cretaceous World, 209–248. The Open University, Cambridge University Press.

KENNEDY, W. J., GALE, A. S., HUBER, B. T., PETRIZZO, M. R., BOWN, P., BARCHETTA, A. and JENKYNS, H. C., 2014. Candidate Global Boundary Stratotype section and point for the base of the Albian Stage: The first appearance of the planktonic foraminiferan *Microhedbergella renilaevis* Huber & Leckie, 2011 in the Marnes Bleues of the Col De Près-Guittard Sectioin, Drôme, France. *Cretaceous Research,* 51: 248–259.

KUMP, L. R. and ARTHUR, M. A., 1999. Interpreting carbon-isotope excursions: carbonates and organic matter. *Chemical Geology* 161:181–198.

LARSON, R. L. and ERBA, E., 1999. Onset of the mid-Cretaceous greenhouse in the Barremian-Aptian: Igneous segments and the biological, sedimentary, and geochemical responses. *Paleoceanography*, 14: 663–678.

LECKIE, R. M., BRALOWER, T. J. and CASHMAN, R., 2002. Oceanic anoxic segments and plankton evolution: Biotic response to tectonic fording during the mid-Cretaceous. *Paleoceanography*, 17: 1–23. 10.1029/2001PA000623.

LONGORIA, J. F., 1974. Stratigraphic, morphologic and taxonomic studies of Aptian planktonic foraminifera. *Revista Espana Micropaleontogia*, Numero Extra, 1–107.

———, 1998. The Mesozoic of the Mexican Cordillera in Nuevo Leon, NE Mexico. In: Longoria, J. F., Krutak, P. R. and Gamper, M. A., Eds., *Geologic Studies in Nuevo Leon, Mexico*. Sociedad Mexicana de Paleontologia, Special Publication, p. 1–44.

MADHAVARAJU, J., SIAL, A. N., CARLOS GONZÁLEZ-LEÓN, C. and NAGARAJAN, R., 2013. Carbon and oxygen isotopic variations in early Albian limestone facies the Mural formation, Pitaycachi section, northeastern Sonora, Mexico. *Revista Mexicana de Ciencias Geológicas*, 30: 526–539.

MENEGATTI, A. P., WEISSERT, H., BROWN, R. S., TYSON, R. V., FARIMOND, P., STRASSER, A. and CARON, M., 1998. High resolution ^{13}C stratigraphy through the early Aptian "Livello Selli" of the Alpine Tethys. *Paleoceanography*, 13: 530–545.

NUÑEZ-USECHE, F., MORENO-BEDMAR, J. A., COMPANY, M. AND BARRAGÁN, R., 2014. A negative carbon isotope excursion within the *Dufrenoyia furcata* Zone: proposal for a new episode for chemostratigraphic correlation in the Aptian. *Carnets de Géologie [Notebooks on Geology],* 14: 129–137.

OGG, J. G., HINNOV, L. A. and HUANG, C., 2012, Cretaceous. In: Gradstein, F. M., Ogg, J. G., Schmitz, M. and Ogg, G., 2012, Eds., *The Geologic Time Geologic Time Scale 2012*. Elsevier B.V., Amsterdam. DOI:10.1016/B978-0-444-59425-9.00027-5.

PETRIZZO, M. R., HUBER, B. T., GALE, A. S., BARCHETTA, A. and JENKYNS, H. C., 2012. Abrupt planktic foraminiferal turnover across the Niveau Kilian at Col de Pré-Guittard (Vocontian Basin, southeast France): new criteria for defining the Aptian/Albian boundary. *Newsletters on Stratigraphy,* 45: 55–74.

QUESNE, D. and FERRY, S., 1995. Detailed relationships between platform and pelagic carbonates (Barremian, SE France). In: House, M.R. and Gale, A.S., Eds., *Orbital forcing timescales and cyclostratigraphy*. Geological Society, Special Publication 85: 165–176.

REBOULET, S., RAWSON, P. F., MORENO-BEDMAR, J. A., AGUIRRE-URRETA, M. B., BARRAGÁN, R., BOGOMOLOV, R., COMPANY, M., GONZÁLEZ-ARREOLA, C., STOYANO-VA, V. I., LUKENEDER, A., MATRION, B., MITTA, V., RANDRIANALY, H., VASICEK, Z., BARABOSHKIN, E. J., BERT, D., BERSAC, S., BOGDANOVA, T. N., BULOT, L. G., LATIO, J.-L., MIKHAILOVA, I. A., ROPOLPO, P. and SZIVES, O., 2010. Report on the 4th International Meeting of the IUGS Lower Cretaceous Ammonite. *Cretaceous Research*, 30: 496–502.

ROBASZYNSKI, F., CARON, M., AMÉDRO, F., DUPUIS, C., HARDENBOL, J., GONZALEZ DONOSO, J. M., LINARES, D. and GARTNER, S., 1993. Le Cénomanien de la région de Kalaat Senan (Tunisie centrale): Litho-biostratigraphie et interprétation séquentielle. *Revue de Paléobiologie*, 12: 351–505.

SALTZMAN, M. R. and THOMAS, E., 2014. Chapter 11 – Carbon isotope stratigraphy. In: Gradstein, F. M., Ogg, J. G., Schmitz, M. D. and Ogg, G. M., Eds., The Geologic Time Scale 2012, Vol. 1, 207–232. Amsterdam, Elsevier.

SANCHEZ-HERNANDEZ, Y. and MAURRASSE, F. J-M. R., 2014a. Geochemical characterization and redox signals from the latest Barremian to the earliest Aptian in a restricted marine basin: El Pui section, Organyà Basin, south-central Pyrenees. *Chemical Geology,* 372: 12–31.

SANCHEZ-HERNANDEZ, Y. and MAURRASSE, F., 2014b. Chemostratigraphy of the Barremian-Aptian El Pui section, Organya Basin, south central Pyrenees, Spain: Environmental conditions associated with carbon isotope segments C2-C6, across OAE1a. *Geological Society of America, Meeting Abstracts, Vancouver, British Colombia*, Paper 176–177.

SCOTT, R. W., 2014. Cretaceous chronostratigraphic database: construction and applications. *Carnets de Geologie [Notebooks on Geology],* 14: 1–13. http://paleopolis.rediris.es/cg/uk-index.html.

SCOTT, R. W., BENSON, D. G., MORIN, R. W., SHAFFER, B. L. and OBOH-IKUENOBE, F. E., 2003. Integrated Albian-Lower Cenomanian chronostratigraphy standard, Trinity River section Texas. In: Scott, R. W., Ed., *U.S. Gulf Coast Cretaceous Stratigraphy and Paleoecology*, 277–334. Perkins Memorial Volume: Gulf Coast Section SEPM Foundation, Special Publications in Geology 1.

SCOTT, R. W., FROST, S. H. and SHAFFER, B. L., 1988. Early Cretaceous sea-level curves, Gulf Coast and southeastern Arabia. In: Wilgus, C. K., Hastings, B. S., Kendall, C. G. St. C., Posamentier, H.

W., Ross, C. A. and Van Wagoner, J. C., Eds., *Sea-level changes: An integrated approach,* 275–284. Tulsa, Society of Economic Paleontologists and Mineralogists (SEPM). Special Publication 42.

SETON, M., GAINA, C., MÜLLER, R. D. AND HEINE, C., 2009. Mid-Cretaceoous seafloor spreading pulse: Fact or Fiction? *Geology*, 37: 687–690.

SLITER, W. V., 1992. Cretaceous planktonic foraminiferal biostratigraphy and paleoceanographic segments in the Pacific Ocean with emphasis on indurated sediment. In: Ishizaki, K. and Saito, T., Eds., *Centenary of Japanese Micropaleontology*, 281–299. Tokyo.

STRASSER, A., CARON, M. and GJERMENI, M., 2001. The Aptian, Albian and Cenomanian of Roter Sattel, Romandes Prealpes, Switzerland; a high-resolution record of oceanographic changes. *Cretaceous Research*, 22: 173–199.

STEIN, M., FÖLLMI, K. B., WESTERMANN, S., GODET, A., ADATTE, T., MATERA, V., FLEITMANN, D., BERNER, Z., 2011. Progressive palaeoenvironmental change during the Late Barremian–Early Aptian as prelude to Oceanic Anoxic Event 1a: Evidence from the Gorgo a Cerbara section (Umbria-Marche basin, central Italy). *Palaeogeography, Palaeoclimatology, Palaeoecology*, 302:396–406.

STEUBER, T., SCOTT, R. W., MITCHELL, S. F. and SKELTON, P. W., 2015. Stratigraphy of Jurassic-Cretaceous genera of the Hippuritida Newell (rudist bivalves). Carter, J., Ed., *Treatise of Invertebrate Paleontology*, in review.

VEIZER, J., ALA, D., AZMY, K., BRUCKSCHEN, P., BUHL, P., BRUHN, F., CARDEN, G. A. F., DIENER, A., EBNETH, S., GODDERIS, Y., JASPER, T., KORTE, C., PAWELLEK, F., PODLAHA, O. G. and STRAUSS, H., 1999. $^{87}Sr/^{86}Sr$, ^{13}C and ^{18}O evolution of Phanerozoic seawater. *Chemical Geology*, 161: 59–88.

WANG, P., TIAN, J. and LOURENS, L. J., 2010. Obscuring of long eccentricity cyclicity in Pleistocene oceanic carbon isotope records. Earth Planetary Science Letters, 290: 319–330 doi:10.1016/j.epsl.2009.12.028

WEISSERT, H. and ERBA, E., 2004. Volcanism, CO_2 and palaeoclimate: a Late Jurassic-Early Cretaceous carbon and isotope record. *Journal of the Geological Society, London*, 161: 695–702.

WEISSERT, H., JOACHIMSKI, M. and SARNTHEIN, M., 2008. Chemostratigraphy. *Newsletters on Stratigraphy*, 42: 145–179.

WENDLER, I., 2013. A critical evaluation of carbon isotope stratigraphy and biostratigraphic implications for Late Cretaceous global correlation. *Earth-Science Reviews*, Amsterdam, vol. 126, p. 116–146.

WENDLER, I., WENDLER, J., GRÄFE, K.-U., LEHMAN, J. and WILLEMS, H., 2009. Turonian to Santonian carbon isotope data from the Tethys Himalaya, southern Tibet. *Cretaceous Research*, 30: 961–979.

WISSLER, L., WEISSERT, H., MASSE, J.-P. and BULOT, L., 2002. Chemostratigraphic correlation of Barremian and lower Aptian ammonite zones and magnetic reversals. *International Journal of Earth Sciences (Geologische Rundschau)*, 91: 272–279.

WISSLER, L., FUNK, H. and WEISSERT, H., 2003. Response of Early Cretaceous carbonate platforms to changes in atmospheric carbon dioxide levels: *Palaoegeography, Palaeoclimatology, Palaeoecology*, 200: 187–205. Doi:10.1016/S0031-0182(03)00450-4.

WISSLER, L, WEISSERT, H., BUONOCUNTO, F.P., FERRERI, V. AND D'ARGENIO, B., 2004. Calibration of the Early Cretaceous time scale: A combined chemostratigraphic and cyclostratigrahic approach to the Barremian-Aptian interval, Campania Apennines and southern Alps (Italy). In: d'Argenio, B., Fischer, A. G., Premoli Silva, I., Weissert, H. and Ferreri, V., Eds., Cyclostratigraphy: Approaches and case histories. *SEPM Special Publication* No. 81: 123–133.

APPENDIX 1
Data Files of chemostratigraphic sections. 'Morph' is a sorting code. Asterix denotes lines not used by GraphCor in the plotting or compositing steps.

Cismon Outcrop Section, Italy (MIDK.26)

Cismon Section, Italy, Lower Cretaceous. Continuous outcrop measured by B. Fouke et al., 1994-5, Vriej Universitat, Amsterdam. Unconformity between 69.01-69.18 at 69.01m. Red Biancone Marker bed 0-6.26 m; Haut/Barrem at 4.9m; Scisti a Fucoidi 47.98-71.62m = 269.0. Channel et al., 1979, Earth & Planet. Sci. Letters 42:133-166; Bralower, 1987, Mar. Micropal. 11:293-310; Erba, 1994; Paleoceanography 9:483-501; Mayer, 1997, Geophysical J. Int. 131:387-400; Erba & Larson, 1998, Riv. Italiana Paleont. Strat. 104:181-192; Channell et al. 2000, GSA Bull. 112:1430-1443.

*Taxa	Morph	Base	Top	
Data from Channell et al. 2000, Table 3 less 35 m adjust to Fouke's measurements				
Magnetochron CM0R	/mb	51	55	
Magnetochron CM1R	/mb	24.58	27.04	
Magnetochron CM3R	/mb	11.56	18.22	
Magnetochron CM6R	/mb	6.61	*	
Magnetochron CM7R	/mb	2.77	5.26	
Magnetochron CM8R	/mb	-16.08	0.75	
Magnetochron CM9R	/mb	*	-24.10	
Carbon peak OAE 2	/gc	128.24	129.5	
Carbon peak OAE 1a	/gc	59	63	
*base-top of inflection of $\delta^{13}C$ curve				
Marker bed Bonarelli	/mb	128.24	128.61	
Marker bed Selli Level	/mb	59	63	
Marker bed Nannoconid crisis	/mb	*	57	
*"Nannoconid crisis" is top of abundance curve below Selli level, Erba '94				
*Top Hauterivian	/ma	*	4.9	
Nanno events taken from Channell et al., 1979, Earth & Planentary Sci. Letter, 42:153-166; depths converted to new measurements.				
Calcicalathina oblongata	/nn	*	93.2	
Eiffellithus turriseiffelii	/nn	70.22	*	
Lithastrinus floralis	/nn	60.44	*	
Prediscosphaera cretacea	/nn	69.20	*	
Nannoconus colomii	/nn	*	50.3	
Nannoconus steinmannii	/nn	*	54.5	
Rucinolithus irregularis	/nn	51	*	
Data from Bralower, 1987, Marine Micropaleo., 11:293-310, Fig. 6; convert depth taking 273m = 51m & 324m = 0m in Fouke's section				
Assipetra infracretacea	/nn	-73.6	62.5	
Calcicalathina oblongata	/nn	-129.5	62.5	
Conusphaera mexicana	/nn	-125.9	60.8	*same as Conusphaera rothii
Cretarhabdus angustiforatus	/nn	-125.9	60.8	
Cretarhabdus conicus	/nn	-84.0	54.6	
Cretarhabdus surirellus	/nn	-125.9	60.8	
Cruciellipsis cuvillieri	/nn	-129.5	-9.5	
Cyclagelosphaera margerelii	/nn	-125.9	60.8	
Diazomatolithus lehmanii	/nn	-129.5	31.1	
Flabellites oblonga	/nn	60.8	*	
Hayesites radiatus	/nn	24.6	59.1	
Helenea chiastia	/nn	-125.9	62.5	
Lithraphidites bollii	/nn	-33.1	3.5	
Lithraphidites carniolensis	/nn	-116.5	60.8	
Manivitella pemmatoidea	/nn	-125.9	62.5	
Markalius circumradiatus	/nn	-122.2	60.8	
Nannoconus bermudezii	/nn	-113.8	60.8	
Nannoconus broennimannii	/nn	54.6	55.8	
Nannoconus bucheri	/nn	-4.0	60.8	
Nannoconus globulus	/nn	-113.8	60.8	
Nannoconus kamptneri	/nn	-36.0	62.5	
Nannoconus steinmannii	/nn	-129.5	62.5	
Nannoconus truitti	/nn	-122.2	60.8	
Parhabdolithus asper	/nn	-125.9	62.5	

APPENDIX 1
continued.

Parhabdolithus embergeri	/nn	-129.5	62.5	
Parhabdolithus splendens	/nn	-84.0	62.5	
Reinhardtites fenestratus	/nn	-73.6	62.5	
Rotelapillus laffittei	/nn	-129.5	60.8	
Rucinolithus irregularis	/nn	53.0	62.5	
Vagalapilla stradneri	/nn	-125.9	62.5	
Watznaueria barnesae	/nn	-129.5	62.5	
Watznaueria communis	/nn	51.1	59.1	
Zygodiscus diplogrammus	/nn	51.1	*	
Zygodiscus elegans	/nn	32.8	60.8	
Data from Nederbragt 1994 personal communication				
Biti breggiensis	/fp	77.5	100.66	
Dica algeriana	/fp	125.77	130.56	
Helv'ana helvetica	/fp	133.1	139.84	
Helv'ana praehelvetica	/fp	131.44	133.1	
Hedb trocoidea	/fp	69.20	107.03	
Leupoldina cabri	/fp	60.44	69.00	
Planomalina buxtorfi	/fp	81.01	101.73	
Rota appenninica	/fp	103.83	120.06	
Rota cushmani	/fp	120.24	128.24	
Rota gandolfi	/fp	111.2	*	
Rota globotruncanoides	/fp	*	125.27	
Rota montsalvensis	/fp	117.11	128.0	
Rota reicheli	/fp	119.86	119.86	
Tici subticinensis	/fp	74.1	92.75	
Tici ticinensis	/fp	76.64	101.73	
Whit archaeocretacea	/fp	128.82	130.56	*ID as Whiteinella spp.

Cismon Cored Section, Italy (MIDK.26B)

Cismon Core, Italy. Middle Aptian to lower Hauterivian section drilled to 131.8 m TD. Aptian/Albian unconformity @ -7.8 m. Channell et al., 2000, Geol. Soc. Am. Bull. 112:1430-1443, figs. 4, 8. Erba & Larson, 1998, Riv. Italiana Paleont. Strat. 104:181-192; Erba et al., 1999, J. Foram. Res., 29:371-391.

*Taxa	Morph	Base	Top(m)	
Magnetochrons; Erba et al., Fig. 5				
Magnetochron CM0R	/mb	-29.17	-25.75	
Magnetochron CM1R	/mb	-56.55	-54.68	
Magnetochron CM3R	/mb	-70.42	-61.7	
Magnetochron CM6R	/mb	-76.1	*	
Magnetochron CM7R	/mb	-78.76	-77.69	
Magnetochron CM8R	/mb	-95.41	-81.14	
Magnetochron CM9R	/mb	*	-105.27	
Marker bed Selli Level	/mb	-23.68	-18.77	
Marker bed Nannoconid crisis	/mb	-23.9	*	
*"Nannoconid crisis" is top of abundance curve below Selli level, Erba '94				
*Top Barremian	/ma	*	-29.17	
*Top Hauterivian	/ma	*	-70	Erba et al., p. 376
Biscutum magnum	/nn	-7.66	*	
Braarudosphaera africana	/nn	-14.28	*	
Calcicalathina oblongata	/nn	*	-68.0	
Corollithion achylosum	/nn	-15.27	*	
Cruciellipsis cuvillieri	/nn	*	-79.19	
Eprolithus floralis	/nn	-19.86	*	
Flabellites oblonga	/nn	-33.48	*	
Lithraphidites bollii	/nn	-116	-71.34	
Nannoconus truitti	/nn	-30.36	*	
Parhabdolithus achlyostaurion	/nn	-4.59	*	
Rucinolithus irregularis	/nn	-32.45	*	
Rucinolithus terebrodentarius	/nn	-82.87	*	Erba et al., p. 378-379
Biti breggiensis	/FP	-4.4	*	
Biti subbreggiensis	/FP	-7.04	*	
Glob'oides aptiense	/FP	-29.06	*	

APPENDIX 1
continued.

Glob'oides blowi	/FP	-60.12	*
Glob'oides ferreolensis	/FP	-29.06	*
Glob'oides maridalensis	/FP	-24.33	*
Glob'oides saundersi	/FP	-18.43	*
*Hedb kutznetsovae	/FP	-64.36	*
Hedb similis	/FP	-64.36	*
Hedb trocoidea	/FP	-18.43	*
Leupoldina cabri	/FP	-24.33	-9.72
Tici praeticinensis	/FP	-7.66	*
Tici primula	/FP	-7.78	*
Tici raynaudi	/FP	-7.04	*
Tici subticinensis	/FP	-0.5	*
Bourkidinium granulatum	/DN	-115	-70
Cassiculosphaeridia reticulata	/dn	*	-7.9
Cymososphaeridium validum	/DN	-115	-83.5
Damassadinium chibane	/DN	-7.7	*
Hystrichosphaeridium atlasiense	/DN	-7.7	*
Hystrichodinium pulchrum	/DN	*	-7.9
Kleithriasphaeridium fasciatum	/DN	-60.9	-59.5 *ID as cf.; acme range
Litosphaeridium arundum	/DN	-2.1	*
Litosphaeridium conispinum	/DN	-2.1	*
Odontochitina operculata	/DN	-53.7	*
Oligosphaeridium totum	/DN	-115	-83.5
Ovoidinium diversum	/DN	-7.7	*
Palaeoperidinium cretaceum	/DN	*	-7.9
Phoberocysta neocomica	/DN	*	-28.1 *top of common occurrence
Pinocchiodinium erbae	/DN	-25.5	-7.9
Prolixosphaeridium conulum	/DN	-7.7	*
Prolixosphaeridium parvispinum	/DN	-56.0	*
Rhynchodiniopsis aptiana	/DN	*	-28.1

MIDK.26C Cismon Core, Italy

Middle Aptian to lower Hauterivian section drilled to 131.8 m TD. Channel et al. 1979, Earth Planetary Science Letters 43:153-166, magnetochrons. Erba et al., 1999, J. Foram. Res., 29:371-391; Depths converted to true stratigraphic thickness: right log, Fig. 2; used in Midk.26B. Aptian/Albian unconformity @ -7.8 m; biostratigraphy Fig. 4. Channell et al., 2000, Geol. Soc. Am. Bull. 112:1430-1443, Figs. 4, 8. *Erba & Larson, 1998, Riv. Italiana Paleont. Strat. 104:181-192. Menegatti et al., 1998, Paleoceanography 13:530-545, Fig. 3 defined CI events.

*Taxa	Morph	Base (m)	Top
*Reversed chrons; Erba et al.,1999, Fig. 5			
Magnetochron CM0R	/mb	-29.17	-25.75
Magnetochron CM1R	/mb	-56.55	-54.68
Magnetochron CM3R	/mb	-70.42	-61.7
Magnetochron CM6R	/mb	-76.1	*
Magnetochron CM7R	/mb	-78.76	-77.69
Magnetochron CM8R	/mb	-95.41	-81.14
Magnetochron CM9R	/mb	*	-105.27
Marker bed Selli Level	/mb	-23.68	-18.77
Marker bed Nannoconid crisis	/mb	-23.9	*
*"Nannoconid crisis" is top of abundance curve below Selli level, Erba '94			
*Top Barremian	/ma	*	-29.17
*Top Hauterivian	/ma	*	-70
*Carbon isotope events Menegatti et al. 1998, Fig. 3; depths Erba et al. 1999, Fig.7			
CI Segment C1	/gc	-38.0	*
CI Segment C2	/gc	-32.0	*
CI Segment C3	/gc	-23.5	*
CI Segment C4	/gc	-22.5	*
CI Segment C5	/gc	-22.0	*
CI Segment C6	/gc	-19.0	*
CI Segment C7	/gc	-18.5	*
CI Segment C8	/gc	-9.0	*

APPENDIX 1
continued.

*Ba Carbon Isotope Segments at Cismon by Wissler et al. 2002,				
*Int. J. Earth Sci 91:272-279, Fig.3; 2003, Palaeo-3 200:187-205, Fig. 7.				
CI Segment A3	/GC	-23.5	*	
CI Segment A2	/GC	-27	*	
CI Segment A1	/GC	-29	*	
CI Segment B8	/GC	-33	*	
CI Segment B7	/GC	-44	*	
CI Segment B6	/GC	-49	*	
CI Segment B5	/GC	-52	*	
CI Segment B4	/GC	-55	*	
CI Segment B3	/GC	-60	*	
CI Segment B2	/GC	-65	*	
CI Segment B1	/GC	-70	*	
*Erba et al., 1999, p. 376				
Biscutum magnum	/nn	-7.66	*	
Braarudosphaera africana	/nn	-14.28	*	
Calcicalathina oblongata	/nn	*	-68.0	
Corollithion achylosum	/nn	-15.27	*	
Cruciellipsis cuvillieri	/nn	*	-79.19	
Eprolithus floralis	/nn	-19.86	*	
Flabellites oblonga	/nn	-33.48	*	
Lithraphidites bollii	/nn	-116.0	-71.34	
Nannoconus truitti	/nn	-30.36	*	
Parhabdolithus achlyostaurion	/nn	-4.59	*	
Rucinolithus irregularis	/nn	-32.45	*	
Rucinolithus terebrodentarius	/nn	-82.87	*	
*Erba et al., 1999, p. 378-379				
Biti breggiensis	/FP	-4.4	*	
Biti subbreggiensis	/FP	-7.04	*	
Glob'oides aptiense	/FP	-29.06	*	
Glob'oides blowi	/FP	-60.12	*	
Glob'oides ferreolensis	/FP	-9.06	*	
Glob'oides maridalensis	/FP	-24.33	*	
Glob'oides saundersi	/FP	-18.43	*	
*Hedb kutznetsovae	/FP	-64.36	*	
Hedb similis	/FP	-64.36	*	
Hedb trocoidea	/FP	-18.43	*	
Leupoldina cabri	/FP	-24.33	-9.72	
Tici praeticinensis	/FP	-7.66	*	
Tici primula	/FP	-7.78	*	
Tici raynaudi	/FP	-7.04	*	
Tici subticinensis	/FP	-0.5	*	
*Erba et al., 1999, p. 380				
Bourkidinium granulatum	/DN	-115.0	-70	
Cassiculosphaeridia reticulata	/dn	*	-7.9	
Cymososphaeridium validum	/DN	-115.0	-83.5	
Damassadinium chibane	/DN	-7.7	*	
Hystrichosphaeridium atlasiense	/DN	-7.7	*	
Hystrichodinium pulchrum	/dn	*	-7.9	
Kleithriasphaeridium fasciatum	/DN	-60.9	-59.5	*ID as cf.; acme range
Litosphaeridium arundum	/DN	-2.1	*	
Litosphaeridium conispinum	/DN	-2.1	*	
Odontochitina operculata	/DN	-53.7	*	
Oligosphaeridium totum	/DN	-115.0	-83.5	
Ovoidinium diversum	/DN	-7.7	*	
Palaeoperidinium cretaceum	/DN	*	-7.9	
Phoberocysta neocomica	/DN	*	-28.1	*top of common occurrence
Pinocchiodinium erbae	/DN	-25.5	-7.9	
Prolixosphaeridium conulum	/DN	-7.7	*	
Prolixosphaeridium parvispinum	/DN	-56.0	*	
Rhynchodiniopsis aptiana	/DN	*	-28.1	

APPENDIX 1
continued.

Roter Sattel, Switzerland (MIDK.98)

Roter Sattel, Romandes Prealps, Switzerland; x° N, y° E, 586.000/159.270.
Cret. Res. 22:173-199, fig. 3. Guillaume, 1986, Fribourg thesis, p. 65, fig. 28; p. 115, fig. 48a;
Base of section at 0 m, top of section at 68 m; Calcaires-Plaquetes Fm.; Intyamon Fm., Couches-Rouges. Fm.

*Taxon name	morph	base	top meters	
Carbon peak OAE 1a	/GC	3.5	6.0	
Carbon peak OAE 1b	/GC	34.9	35.5	
Carbon peak OAE 1c	/GC	37.8	38.7	
Carbon peak OAE 2	/GC	62	64	
Marker bed Selli Level	/mb	4.5	6	
Marker bed Bonarelli	/mb	62	64	
*Black shale intervals marked on fig. 3 by authors				
*Planktic forams by M. Caron				
Biti breggiensis	/fp	37	40.9	
Dica algeriana	/fp	55.2	68	
Dica hagni	/fp	61.4	68	
Glob'oides algerianus	/fp	27.5	31.8	
Glob'oides blowi	/fp	0.2	17.5	
Glob'oides ferreolensis	/fp	24.55	32.3	*top at 32.3 reworked
Hedb infracretacea	/fp	0	54.5	
Hedb planispira	/fp	20.4	54.5	
Hedb sigali	/fp	0	20.2	
Helv'ana helvetica	/fp	67.1	68	
Helv'ana praehelvetica	/fp	61.5	68	*ID as Whiteinella
Leupoldina cabri	/fp	7.4	17.1	
Marginotruncana marianosi	/fp	67.5	68	
Marginotruncana schneegansi	/fp	65.3	68	
Planomalina buxtorfi	/fp	41.1	46.6	
Planomalina cheniourensis	/fp	31.1	31.8	
Planomalina praebuxtorfi	/fp	40.6	41.3	
Rota appenninica	/fp	41.1	54.5	
Rota cushmani	/fp	56.3	61.9	*hardground at 61.95
Rota globotruncanoides	/fp	47.7	54.9	
*Top at hardground at 61.95m too hi, use second LO				
Rota greenhornensis	/fp	50.8	60.6	
Rota montsalvensis	/fp	49.2	60.1	
Rota reicheli	/fp	50.8	58.4	
Tici bejaouaensis	/fp	32.15	32.4	
Tici primula	/fp	36.25	40.2	
Tici subticinensis	/fp	39.6	40.4	
Tici ticinensis	/fp	39.6	46.6	
Whit archaeocretacea	/fp	57.7	68	

Santa Rosa Canyon Section, Mexico (MIDK.3)

Santa Rosa Canyon, Nuevo Leon, Mexico. Blauser & McNulty, 1980, Trans. Gulf Coast Assoc. Geol. Soc., 30:263-272; Ice & McNulty, 1980, idem, 30:403-425. Footage position of stage boundaries projected from experimental graphs. Top La Casita Fm at 24 ft; Top Taraises Fm at 470 ft; Top Lower Tamaulipas Fm at 2500 ft; Top Otates Fm at 2700 ft; Top Upper Tamaulipas Fm at 3195 ft overlain by 30cm blk sh; Top Cuesta del Cura Fm at 3745-3770 ft in covered interval; Top of section in Agua Nueva Fm at 4293 ft.

*Taxon name	morph	base	top feet
Top Berriasian	/ma	400	400
Top Valanginian	/ma	1140	1140
Top Hauterivian	/ma	1700	1700
Top Aptian	/ma	2710	2710
Top Early Albian	/ma	3000	3000
Top Albian	/ma	3575	3575
Marker bed Al SB WA 1	/mb	3195	3195
Marker bed Ap SB PR 1	/mb	2500	2500

APPENDIX 1
continued.

Olcostephanus coahuilaensis	/am	429	429	
Neocomites sp.	/am	429	429	
*ID by K. Young in Blauser, 1981, p. 42, West Tx. Geol. Soc. Guidebook Publ. 81-74;				
Calpionella alpina	/ca	20	49	
Calpionella elliptica	/ca	20	197	
Calpionella oblonga	/ca	49	436	
Calpionella simplex	/ca	118	197	
Calpionellites darderi	/ca	295	295	*ID as Calpionella darderi
Remaniella cadischiana	/ca	39	49	
Stenosemellopsis hispanica	/ca	295	295	
Tintinopsella carpathica	/ca	20	463	
Tintinopsella longa	/ca	49	410	
Nannoconus steinmannii	/nn	39	2258	
Nannoconus wassallii	/nn	2460	2558	
Bonetocardiella conoidea	/ca	3395	4023	
Colomiella mexicana	/ca	2676	2808	
Colomiella recta	/ca	2676	3011	
Microcalamoides diversus	/id	2676	3198	
Pith ovalis	/ca	3395	3395	
Pith sphaerica	/ca	3198	4023	
Biti breggiensis	/fp	3211	3415	
Glob'oides algerianus	/fp	2519	2538	
Glob'oides bentonensis	/fp	3467	3742	
Glob'oides cushmani	/fp	3461	4129	
Hedbergella washitensis	/fp	2676	3447	
Helv'ana helvetica	/fp	4211	4211	
Marginotruncana schneegansi	/fp	4244	4244	
Planomalina buxtorfi	/fp	3421	3493	
Praeglobotruncana delrioensis	/fp	3447	3742	
Praeglobotruncana stephani	/fp	3447	4096	
Rota appenninica	/fp	3428	3742	
Rota cushmani	/fp	4031	4129	
Rota gandolfi	/fp	3900	3900	
Rota greenhornensis	/fp	3949	3949	
Tici roberti	/fp	3198	3480	
Tici subticinensis	/fp	3224	3410	
Tici ticinensis	/fp	3326	3493	

Santa Rosa Canyon Section, Mexico (MIDK.3B)

Santa Rosa Canyon, Nuevo Leon, Mexico. Blauser & McNulty, 1980, Trans. Gulf Coast Assoc. Geol. Soc., 30:263-272; Ice & McNulty, 1980, idem, 30:403-425. New Nanno data from Bralower et al., 1999, J. Foram Research, Fig. 3. Lithostratigraphy same as in MIDK.3.

*Taxon name	morph code	base	top ft	
Top Berriasian	/ma	400	400	
Top Valanginian	/ma	1140	1140	
Top Hauterivian	/ma	1700	1700	
Top Barremian	/ma	2210	2210	
Top Aptian	/ma	2710	2710	
Marker bed Ap SB PR 1	/mb	2500	2500	
Olcostephanus coahuilaensis	/am	429	429	
Neocomites sp.	/am	429	429	
*ID by K. Young in Blauser, 1981, p. 42, West Tx. Geol. Soc. Guidebook Publ. 81-74;				
Calpionella alpina	/ca	20	49	
Calpionella elliptica	/ca	20	197	
Calpionella oblonga	/ca	49	436	
Calpionella simplex	/ca	118	197	
Calpionellites darderi	/ca	295	295	*ID as Calpionella darderi
Remaniella cadischiana	/ca	39	49	
Stenosemellopsis hispanica	/ca	295	295	
Tintinopsella carpathica	/ca	20	463	
Tintinopsella longa	/ca	49	410	

APPENDIX 1
continued.

Nannoconus steinmannii	/nn	39	2258
Nannoconus wassallii	/nn	2460	2558
Bonetocardiella conoidea	/ca	3395	4023
Colomiella mexicana	/ca	2676	2808
Colomiella recta	/ca	2676	3011
Microcalamoides diversus	/id	2676	3193
Pith ovalis	/ca	3395	3395
Pith sphaerica	/ca	3198	4023
Biti breggiensis	/fp	3211	3415
Glob'oides algerianus	/fp	2519	2538
Glob'oides bentonensis	/fp	3467	3742
Glob'oides cushmani	/fp	3461	4129
Hedbergella washitensis	/fp	2676	3447
Helv'ana helvetica	/fp	4211	4211
Marginotruncana schneegansi	/fp	4244	4244
Planomalina buxtorfi	/fp	3421	3493
Praeglobotruncana delrioensis	/fp	3447	3742
Praeglobotruncana stephani	/fp	3447	4096
Rota appenninica	/fp	3428	3742
Rota cushmani	/fp	4031	4129
Rota gandolfi	/fp	*	3900
Rota greenhornensis	/fp	3949	3949
Tici roberti	/fp	3198	3480
Tici subticinensis	/fp	3224	3410
Tici ticinensis	/fp	3326	3493
*Data from Bralower et al., 1999, fig. 7			
Carbon peak OAE 1b	/gc	2791.9	2828.0
Carbon peak OAE 1a	/gc	2516.4	2565.6
*base-top of inflection of $\delta^{13}C$ curve			
Marker bed Nannoconid crisis	/mb	2483.3	2540.0
*"Nannoconid crisis" is top of abundance curve below Selli level, Erba '94			
*Nanno events taken from Bralower et al., 1999, J. Foram Research, 29(4), Fig. 3;			
*convert meter position to feet and add 2073.6'; base La Pena/Otates at 130 m (426.4') = 2500'			
Assipetra infracretacea	/nn	2406.8	3091.4
Bidiscus rotatorius	/nn	2586.3	3101.2
Biscutum constans	/nn	2515.4	3111.1
Braarudosphaera regularis	/nn	2406.8	3130.7
Chiastozygus litterarius	/nn	2539.4	2539.4
Corollithion achylosum	/nn	2614.1	2813.6
Cretarhabdus conicus	/nn	2515.4	2825.7
Cretarhabdus surirellus	/nn	2482.9	3101.2
Cribrosphaerella ehrenbergii	/nn	2791.3	2791.3
Cyclagelosphaera margerelii	/nn	2442.9	3111.1
Diazomatolithus lehmanii	/nn	2511.5	3111.1
*Eiffellithus turriseiffelii	/nn	3071.7	3111.1
*This report extends into M. Albian; lowest base at 2633.8' too low			
Eprolithus floralis	/nn	2540.7	3145.5
Flabellites oblonga	/nn	2527.9	3101.2
Hayesites albiensis	/nn	3101.2	3111.1
*Lithraphidites alatus	/nn	2614.1	2614.1 *ID as subspecies magnus
Helenea chiastia	/nn	2482.9	3101.2
Lithraphidites carniolensis	/nn	2442.9	3101.2
Manivitella pemmatoidea	/nn	2511.1	3101.2
Markalius circumradiatus	/nn	2538.4	3101.2
Micrantholithus hoschulzii	/nn	2448.2	2646.0
Micrantholithus obtusus	/nn	2527.9	2586.3
Nannoconus bermudezii	/nn	2425.2	2425.2
Nannoconus bucheri	/nn	2539.4	2543.6
Nannoconus globulus	/nn	2627.9	2627.9
Nannoconus kamptneri	/nn	2425.2	2623
Nannoconus steinmannii	/nn	2405.8	2482.9
Nannoconus truitti	/nn	2543.6	3111.1

APPENDIX 1
continued.

*Nannoconus wassalii	/nn	2511.5	2614.1
Parhabdolithus achlyostaurion	/nn	2527.9	3111.1
Percivalia fenestrata	/nn	2611.2	3101.2
Prediscosphaera columnata	/nn	2786.3	2938.9
Rhagodiscus angustus	/nn	2627.9	2786.3
Rhagodiscus asper	/nn	2539.4	3111.1
Rhagodiscus splendens	/nn	2538.4	3101.2
Rotelapillus laffittei	/nn	2515.4	3101.2
Rucinolithus irregularis	/nn	2425.2	3130.7
Rucinolithus terebrodentarius	/nn	2477.7	3101.2
Tranolithus orionatus	/nn	2909.3	3130.7
Vagalapilla stradneri	/nn	2562.0	2562.0
Watznaueria barnesae	/nn	2409.5	3145.5
Watznaueria britannica	/nn	2539.4	2539.4
Watznaueria communis	/nn	2540.7	2791.3
Zeugrhabdotus embergeri	/nn	2440.6	3145.5
Zeugrhabdotus erectus	/nn	3101.2	3111.1
Zygodiscus diplogrammus	/nn	2482.9	3130.7
Zygodiscus elegans	/nn	2527.9	2938.9 *base @ 2633.8' too low
*Organic Carbon isotope events defined by inflection points at base; measured on fig. 7 converted to ft plus 2073.6ft			
CI Segment C15	/gc	3060.0 *	*slight increase @ 986.4m
CI Segment C14	/gc	3020.3 *	*sharp decrease @ 946.7
CI Segment C13	/gc	2837.6 *	*fairly constant beginning @ 764.0
CI Segment C12	/gc	2822.4 *	*sharp increase @ 748.8
CI Segment C11	/gc	2788.6 *	*sharp decrease @ 715.0
CI Segment C10	/gc	2723.6 *	*plateau beginning @ 650.0
CI Segment C9	/gc	2712.2 *	*sharp increse @ 638.6
CI Segment C8	/gc	2692.4 *	*sharp decrese @ 618.8
CI Segment C7	/gc	2593.6 *	*plateau beginning @ 520.0
CI Segment C6	/gc	2582.2 *	*increase @ 508.6
CI Segment C5	/gc	2538.4 *	*constant beginning @ 464.8
CI Segment C4	/gc	2528.6 *	*sharp increase @ 455.0
CI Segment C3	/gc	2523.1 *	*sharp decrease @ 449.5
CI Segment C2	/gc	2477.9 *	*moderate decrease @ 404.3
CI Segment C1	/gc	2398.6 *	*plateau beginning @ 325.0

Santa Rosa Canyon, Nuevo Leon, Mexico (MIDK.3c)

Bralower et al., 1999; Compare with Midk3 & Midk.3b. Composted section of three separate sample segments: SRA 0-97m; SRB 97-209m w/ gap at 127-134m; SRC 209-330m. Contact of San Angelo/La Peña=Otates at 130m; Base Lower Tamaulipas Fm at 210m; Top of section in Tamaulipas Fm at 330m.

Taxon name	Morph code	Base	Top meters
	Bralower et al., 1999, fig. 7		
Carbon peak OAE 1b	/gc	219	234
Carbon peak OAE 1a	/gc	130	150
*base-top of inflection of $\delta^{13}C$ curve			
Marker bed Niveau Jacob	/mb	192	195 (RWS interpretation)
*Nanno events from Bralower et al., 1999, J. Foram Research, 29(4), Fig. 3;			
Marker bed Nannoconid crisis	/mb	124.9	142.2
*Nannoconid crisis, Table 2 is top of abundance curve below Selli level, Erba '94			
Assipetra infracretacea	/nn	101.6	310.3
Bidiscus rotatorius	/nn	156.3	313.3
Biscutum constans	/nn	134.7	316.3
Braarudosphaera regularis	/nn	138.5	322.3
Chiastozygus litterarius	/nn	142.4	142.4
Corollithion achylosum	/nn	164.8	225.6
Cretarhabdus conicus	/nn	133.5	229.3
Cretarhabdus surirellus	/nn	124.8	313.3
Cribrosphaerella ehrenbergii	/nn	218.8	218.8
Cyclagelosphaera margerelii	/nn	112.6	316.3
Diazomatolithus lehmanii	/nn	133.5	316.3

APPENDIX 1
continued.

Eiffellithus monechiae	/nn	313.3	313.3	*base at 225.6 too low
Eiffellithus turriseiffelii	/nn	304.3	316.3	*lowest base at 170.8 too low
Eprolithus floralis	/nn	142.4	326.8	
Flabellites oblonga	/nn	138.5	313.3	
Hayesites albiensis	/nn	313.3	316.3	
*Lithraphidites alatus	/nn	164.8	164.8	*ID as subspecies magnus
Lithraphidites carniolensis	/nn	112.6	313.3	
Manivitella pemmatoidea	/nn	133.5	313.3	
Markalius circumradiatus	/nn	141.7	313.3	
Micrantholithus hoschulzii	/nn	114.2	174.5	
Micrantholithus obtusus	/nn	138.5	156.3	
*Micrantholithus speetonensis	/nn	159.4	159.4	too young
Microstaurus chiastius	/nn	124.8	225.6	*Top at 313.3 too high
Nannoconus bermudezii	/nn	107.2	107.2	
Nannoconus bucheri	/nn	142.0	143.3	
Nannoconus globulus	/nn	169.0	169.0	
Nannoconus kamptneri	/nn	107.2	167.5	
Nannoconus steinmannii	/nn	101.3	124.8	
Nannoconus truitti	/nn	143.3	316.3	
Nannoconus wassalii	/nn	133.5	164.8	
Parhabdolithus achlyostaurion	/nn	138.5	316.3	
Percivalia fenestrata	/nn	163.9	313.3	
Prediscosphaera columnata	/nn	217.3	263.8	
Rhagodiscus angustus	/nn	169.0	217.3	
Rhagodiscus asper	/nn	142.4	316.3	
Rhagodiscus splendens	/nn	141.7	313.3	
Rotelapillus laffittei	/nn	133.5	313.3	
Rucinolithus irregularis	/nn	107.2	322.3	
Rucinolithus terebrodentarius	/nn	123.2	313.3	
Tranolithus orionatus	/nn	254.8	322.3	
Vagalapilla stradneri	/nn	138.5	316.3	
Watznaueria barnesae	/nn	101.3	326.8	
Watznaueria britannica	/nn	142.0	142.0	
Watznaueria communis	/nn	142.4	218.8	
Watznaueria ovata	/nn	225.6	225.6	
Zeugrhabdotus embergeri	/nn	111.9	326.8	
Zygodiscus diplogrammus	/nn	124.8	322.3	
Zygodiscus elegans	/nn	138.5	263.8	
Zygodiscus erectus	/nn	170.8	178.6	*Top at 316.3 too high
*Planktic forams by W. Sliter, p. 425				
Clav simplex	/fp	299.8	299.8	*ID as cf.
Favusella washitensis	/fp	214.3	207.4	*ID as "favusellids"
Glob'oides algerianus	/fp	181.1	197.6	
Glob'oides blowi	/fp	101.3	101.3	
Glob'oides ferreolensis	/fp	159.7	172.7	
Leupoldina cabri	/fp	146.0	154.3	
Tici primula	/fp	329.8	329.8	
Tici roberti	/fp	329.8	329.8	
Colomiella mexicana	/ca	207.4	207.4	*Blauser & McNulty, 1980
Colomiella recta	/ca	207.4	207.4	
*Organic Carbon isotope events defined by inflection points at base (Fig. 7)				
CI Segment C15	/gc	303	*	*slight increase
CI Segment C14	/gc	291	*	*sharp decrease
CI Segment C13	/gc	236	*	*begin fairly constant
CI Segment C12	/gc	230	*	*sharp increase
CI Segment C11	/gc	220	*	*sharp decrease
CI Segment C10	/gc	200	*	*begin plateau
CI Segment C9	/gc	198	*	*sharp increase
CI Segment C8	/gc	190	*	*sharp decrease
CI Segment C7	/gc	160	*	*begin plateau
CI Segment C6	/gc	156	*	*increase
CI Segment C5	/gc	143	*	*begin constant
CI Segment C4	/gc	140	*	*sharp increase

APPENDIX 1
continued.

CI Segment C3	/gc	138	*	*sharp decrease
CI Segment C2	/gc	120	*	*moderate decrease
CI Segment C1	/gc	100	*	*begin plateau

Angles section, Vocontian Basin, France (MIDK.120)

Angles section, Vocontian Basin, France. Oosting et al., 2006, Cret. Res. 27:792-813, Fig. 3.
Reference section for Barremian/Aptian boundary. Alternating limestone/marl continuous deposition.

*Taxa	Morph Gp	Base	Top m	
*Dinoflagellates by Oosting et al., 2006, Cret. Research 27:792-813, Table 2				
Batioladinium micropodum	/dn	79.0	83.9	
Callaiosphaeridium asymmetricum	/dn	70.3	83.9	
Cassiculosphaeridia magna	/dn	70.3	74.0	
Cassiculosphaeridia reticulata	/dn	70.3	83.9	
Cerbia tabulata	/dn	70.3	83.9	
Cometodinium comatum	/dn	70.3	83.9	
Cometodinium habibii	/dn	70.3	83.9	
Coronifera albertii	/dn	72.9	72.9	
Coronifera oceanica	/dn	70.3	83.9	
Cribroperidinium tenuiceras	/dn	81.5	83.9	
Ctenidodinium elegantulum	/dn	70.3	83.9	
Cyclonephelium intonusum	/dn	74.0	83.9	
Cymososphaeridium validum	/dn	73.5	81.5	
Dingodinium cerviculum	/dn	71.0	83.9	
Dingodinium europaeum	/dn	71.0	71.0	
Discorsia nanna	/dn	71.0	72.9	
Dissiliodinium globulum	/dn	70.3	83.9	
Druggidium apicopaucicum	/dn	70.3	75.5	
Druggidium deflandrei	/dn	71.0	83.9	
Elytrocysta circulata	/dn	74.0	83.9	
Exochosphaeridium phragmites	/dn	70.3	83.9	
Florentinia cooksoniae	/dn	72.0	79.0	
Florentinia interrupta	/dn	72.9	83.9	
Florentinia mantellii	/dn	71.0	82.0	
Gardodinium trabeculosum	/dn	71.0	83.9	
Heslertonia heslertonensis	/dn	70.3	83.9	
Heterosphaeridium heteracanthum	/dn	70.3	83.9	
Hystrichodinium pulchrum	/dn	70.3	83.9	
Hystrichosphaeridium recurvatum	/dn	72.0	83.9	
Hystiocysta outananensis	/dn	70.3	83.9	
Kleithriasphaeridium eoinodes	/dn	70.3	83.9	
Kleithriasphaeridium fasciatum	/dn	*	47.5	*Based on Fig. 5
Meiourogonyaulax stoveri	/dn	70.3	83.9	
Muderongia simplex	/dn	70.3	74.0	
Muderongia staurota	/dn	70.3	70.3	
Occisucysta tentorium	/dn	75.5	83.9	
Odontochitina operculata	/dn	44.5	83.9	
Oligosphaeridium complex	/dn	70.3	83.9	
Ovoidinium diversum	/dn	72.0	83.9	
Palaeoperidinium cretaceum	/dn	70.3	83.9	
Pareodinia ceratophora	/dn	70.3	79.6	
Phoberocysta neocomica	/dn	70.3	83.9	
Phoberocysta tabulata	/dn	72.9	83.9	
Prolixosphaeridium parvispinum	/dn	46.0	83.1	
Protoellipsodinium touile	/dn	72.9	72.9	
Pseudoceratium pelliferum	/dn	70.3	75.5	
Pseudoceratium retusum	/dn	72.9	83.9	
Pseudoceratium retusum var. securigerum	/dn	79.0	83.9	
Rhynchodiniopsis fimbriata	/dn	70.3	83.9	
Scriniodinium? campanula	/dn	71.0	83.9	
Tehamadinium coummia	/dn	81.5	81.5	
Tehamadinium sousense	/dn	72.9	83.9	

APPENDIX 1
continued.

Trichodinium castanea	/dn	70.3	83.9
Wallodinium krutzschii	/dn	70.3	82.0
Wrevittia cassidata	/dn	71.0	83.9
Wrevittia helicoidea	/dn	70.3	83.9
*Ammonites based on Oosting et al., p. 795, Fig. 3 from Busnardo 1965			
Colchidites sp.	/am	69	74
Deshayesites tuarkyricus	/am	80	84
Deshayesites weissi	/am	85	*
Martelites sarasini	/am	69	74

Alvier section, Swiss Alps (MIDK.146)

*Wissler et al., 2003, Palaeo-3, 200:187-205, Fig. 3. Base of section at 0 m condensed glauconite bed w/ Haut-Barrem ammonites: angulicostata & caillaudianus. Top beds overlain by phosphorite w/ Upper Aptian *C. crassicostatum* & *P. melchiorisl;*
Carbon Isotope Segments at Cismon by Wissler et al. 2003, Fig. 3, Palaeo-3

*TAXA	Morph	Top meters	
CI Segment A1	/GC	360	*
CI Segment B8	/GC	330	*
CI Segment B7	/GC	260	*
CI Segment B6	/GC	205	*
CI Segment B5	/GC	160	*
CI Segment B4	/GC	90	*
CI Segment B3	/GC	20	*

Churfirsten section, Swiss Alps (MIDK.147)

*Wissler et al., 2003, Palaeo-3, 200:187-205, Fig. 5. Base of section at 0 m covered. Hardground at 105m; *Praecaprina* at 211m; top overlain by unconformity. Carbon Isotope Segments at Cismon by Wissler et al. 2003, Fig. 5, Palaeo-3

*TAXA	Morph	Top meters	
CI Segment A2	/GC	180	*
CI Segment A1	/GC	155	*
CI Segment B8	/GC	150	*
CI Segment B7	/GC	110	*
CI Segment B6	/GC	105	*
CI Segment B5	/GC	80	*

Resolution Guyot, Mid Pacific Ocean (Midk.407)

Resolution Guyot 21°20'N, 174°20'E, ODP Leg 62, site 866.
JENKYNS, H.C., 1995, 6. Carbon-isotope stratigraphy and paleoceanographic significance of the Lower Cretaceous shallow-water carbonates of Resolution Guyot, Mid-Pacific Mountains, in Winterer, E., Sager, W.W., Firth, J.V., and Sinton, J.M., eds., Proceedings of the Ocean Drilling Program, Scientific Results, vol. 143: 99-104. JENKYNS, H.C. and WILSON, P.A., 1999, Stratigraphy, paleoceanography, and evolution of Cretaceous Pacific guyots: Relics from a Greenhouse Earth: American Journal of Science: 299:341-392. Core 0 to 1743.6 mbsf; basalt top at 1620 dated at 127.6 +/- 2.1 Ma (p. 352) 128+/-2 to 99 +/- 2 Ma Gradstein 1994 scale. Base Barrem @1400, base Aptian @ 900; base Albian @400 by Sr 87/87 fig. 5; Incomplete sedimentary record with calcretes 450-300 mbsf; possible strat gaps at 820 & 640 mbsf; Biostrat FOs (fig. 6, 1999): *blowi* ~900, *cabri* @750, *ferreolensis* @580, *algerianus* @520, Selli @860-800 in cyclic pkst-wkst & algal lamintes w/ clay/organic-rich intervals. Top picks lower in fig. 6 & fig. 7, 1995)

*TAXA	MORPH	BASE	TOP mbsf
*B1 to 3 older than age of basalt at TD			
CI Segment B4	/gc	1580	***
CI Segment B5	/gc	1490	***
CI Segment B6	/gc	1410	***
CI Segment B7	/gc	1275	***
CI Segment B8	/gc	1100	***
CI Segment C1	/gc	1180	***
CI Segment C2	/gc	1080	***
CI Segment C3	/gc	850	***

APPENDIX 1
continued.

```
CI Segment C4   /gc         840   ***
CI Segment C5   /gc         830   ***
CI Segment C6   /gc         780   ***
CI Segment C7   /gc         680   ***
CI Segment C8   /gc         580   ***
CI Segment C9   /gc         470   ***
CI Segment C10   /gc        400   ***
CI Segment C11   /gc       330   ***
CI Segment C12   /gc       290   ***
CI Segment C13   /gc       210   ***
CI Segment C14   /gc         90   ***
*unconformity @ 20mbsf CI Segment C15   /gc
*foram FOs predicted by projection to carbon 13 curve (Jenkyns 1995 fig.6)
Glob'oides algerianus      /fp    530   ***
Glob'oides blowi           /fp    900   ***
Glob'oides ferreolensis    /fp    680   ***
Leupoldina cabri           /fp    750   ***
Marker bed Selli Level     /mb    860   800
*In cyclic pkst-wkst & algal lamintes w/ clay/organic-rich intervals

Explanation of Morph - Morphologic Codes:
Am=ammonites; ca=calcispheres; DN/dn=dinoflagellates; FP/fp=planktic foraminifers;
GC/gc=geochemical markers; id=indeterminate organism; mb=marker beds;
NN/nn=nannoplankton.
```